The Journal of Immunology

Development of Neutralizing Multimeric Nanobody Constructs Directed against IL-13: From Immunization to Lead Optimization

This information is current as of December 8, 2021.

Philippe J.-L. Y. Gevenois, Pieter De Pauw, Steve Schoonooghe, Cédric Delporte, Thami Sebti, Karim Amighi, Serge Muyldermans and Nathalie Wauthoz

---

References   This article **cites 79 articles**, 18 of which you can access for free at:
http://www.jimmunol.org/content/207/10/2608.full#ref-list-1

Why *The JI*? Submit online.

- **Rapid Reviews! 30 days*** from submission to initial decision

- **No Triage!** Every submission reviewed by practicing scientists

- **Fast Publication!** 4 weeks from acceptance to publication

*average

Subscription   Information about subscribing to *The Journal of Immunology* is online at:
http://jimmunol.org/subscription

Permissions   Submit copyright permission requests at:
http://www.aai.org/About/Publications/JI/copyright.html

Email Alerts   Receive free email-alerts when new articles cite this article. Sign up at:
http://jimmunol.org/alerts

Development of Neutralizing Multimeric Nanobody Constructs Directed against IL-13: From Immunization to Lead Optimization

Philippe J.-L. Y. Gevenois,* Pieter De Pauw,[†] Steve Schoonooghe,[‡] Cédric Delporte,[§] Thami Sebti,[¶] Karim Amighi,* Serge Muyldermans,[†] and Nathalie Wauthoz*

IL-13 is a pleiotropic cytokine mainly secreted by Th2 cells. It reacts with many different types of cells involved in allergy, inflammation, and fibrosis, e.g., mastocytes, B cells, and fibroblasts. The role of IL-13 in conditions involving one or several of these phenotypes has therefore been extensively investigated. The inhibition of this cytokine in animal models for various pathologies yielded highly promising results. However, most human trials relying on anti–IL-13 conventional mAbs have failed to achieve a significant improvement of the envisaged disorders. Where some studies might have suffered from several weaknesses, the strategies themselves, such as targeting only IL-13 using conventional mAbs or employing a systemic administration, could be questioned. Nanobodies are recombinant Ag-binding fragments derived from the variable part of H chain–only Abs occurring in Camelidae. Thanks to their single-domain structure, small size ($\approx$15 kDa), good stability, and solubility, they can be engineered into multispecific constructs for combined therapies or for use in new strategies such as formulations for local administration, e.g., pulmonary administration. In this study, we describe the generation of 38 nanobodies that can be subdivided into five CDR3 families. Nine nanobodies were found to have a good affinity profile (K_D = 1–200 nM), but none were able to strongly inhibit IL-13 biological activity in vitro (IC$_{50}$ > 50 μM: HEK-Blue IL-13/IL-4 cells). Multimeric constructs were therefore designed from these inhibitors and resulted in an up to 36-fold improvement in affinity and up to 300-fold enhancement of the biological activity while conserving a high specificity toward IL-13. *The Journal of Immunology*, 2021, 207: 2608–2620.

Interleukin-13 is a pleiotropic cytokine whose mature form consists of a glycosylated protein of 122 aa (1) with an m.w. of 13,300 (2). This cytokine is recognized by two receptors. The first one is a heterodimeric receptor whereby IL-13 first binds to the IL-13Rα_1 subunit with a low-to-moderate affinity (K_D = 2–10 nM) (3–6). The complex then recruits human IL-4R, resulting in the formation of the active complete receptor, which has a higher affinity for IL-13 (32–400 pM) (5–7). Most of the biological activity of IL-13 is mediated by its binding through this receptor. Loading this receptor with IL-13 will lead to the secretion of proinflammatory cytokines and chemokines, the recruitment of inflammatory cells, the activation of B cells, or Ig isotype switching to IgE (8, 9). The second known receptor of IL-13, IL-13Rα_2, is monomeric but exhibits a much higher affinity for IL-13 (0.16–50 pM) (4, 6). IL-13Rα_2 was long considered to be a decoy receptor whose biological activity was thought to downregulate IL-13 signaling (4). However, more recent studies have shown that IL-13Rα_2 may also lead to functional activity (10, 11). Because of the high number of its plausible effects in inflammatory and fibrotic functions, many preclinical studies involving the inhibition of IL-13 have already been conducted. These studies have shown promising results for many pathologic

conditions, such as asthma (3, 12–19), atopic dermatitis (20, 21), idiopathic pulmonary fibrosis (22), hepatic fibrosis (23), systemic sclerosis (24–26), ulcerative colitis (27), eosinophilic esophagitis (28, 29), and different types of cancers (30–33).

Further to those encouraging preclinical results, six anti–IL-13 mAbs have been tested in clinical trials so far, mostly involving inflammatory and/or fibrotic pathologies. The most successful trials were those investigating anti–IL-13 therapy for moderate-to-severe atopic dermatitis. Two mAbs, lebrikizumab and tralokinumab, showed very promising results as they are both currently under development in phase III clinical trials and predicted to be marketed soon. Despite the failure of the first mAb (dectrekumab) tested for eosinophilic esophagitis (34, 35), another anti–IL-13 mAb (cendakimab) reached its primary end point (mean esophageal eosinophil count in the five high-power fields) and is currently being considered for this disease (36). In contrast, studies against asthma did not encounter the same success (37–41) despite it being the most investigated disease for anti–IL-13 therapies (with five out of the six anti–IL-13 mAbs that were assessed for clinical trials). The most promising Ab was lebrikizumab, which significantly reduced the rate of asthma exacerbation rate in the treated groups compared with the

*Unit of Pharmaceutics and Biopharmaceutics, Free University of Brussels, Faculty of Pharmacy, Brussels, Belgium; [†]Laboratory of Cellular and Molecular Immunology, Free University of Brussels, Ixelles, Belgium; [‡]Flemish Institute for Biotechnology Nanobody Core, Free University of Brussels, Brussels, Belgium; [§]Unit of Pharmacognosy, Bioanalysis and Drug Discovery, RD3 and Analytical Platform of the Faculty of Pharmacy, Free University of Brussels, Brussels, Belgium; and [¶]S.M.B. Laboratories, Brussels, Belgium

ORCIDs: 0000-0002-5202-5504 (P.J.-L.Y.G.); 0000-0002-6463-4585 (P.D.P.); 0000-0001-7453-7028 (C.D.); 0000-0002-3678-3575 (S.M.); 0000-0003-2445-5790 (N.W.).

placebo group (primary end point) during its phase II and one of its phase III trials for moderate-to-severe asthma. However, it failed to confirm these results during the replicate of its phase III trial. Because of these inconsistent results, its development was withdrawn for this application (38). Despite these failures to consistently reduce the asthma exacerbation rate within trials, a significant clinical improvement was consistently reported for secondary outcomes such as the forced expiratory volume in 1 s for both lebrikizumab (38) and tralokinumab (42). Other indications such as idiopathic pulmonary fibrosis, chronic obstructive pulmonary disease, Hodgkin lymphoma, alopecia areata, ulcerative colitis, and systemic sclerosis have also been tested for anti−IL-13 therapy. However, none of the assessed mAbs showed the expected improvement for their targeted condition (43−49).

Despite the huge potential demonstrated in preclinical studies in animal models, anti−IL-13 therapies have not achieved their expected success. This is especially true for asthma, even if meaningful clinical improvements have been noticed. Reasons could lie in the study design, as the authors of some trials acknowledged that their studies might have inherent limitations that could partially explain the failures (38, 42), or that the primary outcome may not have been adequately chosen (34). However, the initial strategy might also be questioned. For instance, it might be more interesting for asthma therapy to use the pulmonary route instead of s.c. or i.v. injection. Indeed, mAbs are relatively complex proteins of high m.w., which might be quite challenging to stabilize for these routes of administration. Omalizumab, an anti-IgE used for asthma therapy, has already undergone attempts for administering via the pulmonary route instead of s.c. injections. Nevertheless, adequate aerodynamic behavior could only be obtained at the limit of its stability (50, 51). The use of Ab fragments may also be a solution. Such a possibility has already been envisaged by Hacha et al. (15) using a Fab from a conventional mAb (Fab′). This approach showed promising results in a mouse model, with superior results for the pulmonary route over the i.v. route (15). However, a Fab′ still consists of a multidomain protein with a relatively high m.w. (55,000), linked by disulfide bridges. More recently, atypic Abs that lack L chains were discovered in Camelidae species. Nanobodies (Nbs) are the isolated variable fragment of these Abs. They consist of the smallest and simple Ab fragment that retains full binding activity and that does not require sequence modification (i.e., unlike single-chain variable fragments, which need a synthetic linker). Nbs present massive advantages compared with conventional Abs and their fragments. They are 10-fold smaller (m.w. ≈15 kDa, 15,000) than mAbs and consist of a single domain protein, which is highly amenable for engineering, for instance into multivalent or multiparatopic constructs. In contrast to an isolated H chain of the variable fragments of conventional Igs, Nbs are strictly monomeric and highly soluble in aqueous solutions as they lack the hydrophobic surface at the region where the variable domain of the H chain interacts with the variable domain of the L chain of conventional Igs (52). Furthermore, Nbs are easy to produce in microorganisms (52). Multiple applications using Nbs have been explored (53), and a first drug for humans, consisting of a multimeric Nb administered by i.v. injection (54), was approved by the European Medicines Agency in 2018 and the U. S. Food and Drug Administration in 2019 (55).

The aim of this study was to identify anti-human IL-13 Nbs that prevented the binding of IL-13 to its receptors and to optimize their biological activity by combining the most active monomeric subunit (-s) into multimeric constructs.

Materials and Methods

Identification of rIL-13−specific Nb

The generation of Nbs was performed as previously described (56). Briefly, two llamas received weekly s.c. injections (for 3 wk), either with 85 or 165 μg of glycosylated soluble human rIL-13 (catalog [Cat.] no. 10369-HNAC, Sino Biological, Beijing, China) emulsified in Gerbu LQ3000 (Cat. no. 30000025, GERBU Biotechnik, Heidelberg, Germany). The Nb-encoding genes from the PBLs of llamas were amplified by PCR before being ligated into the phagemid vector pMECs and transformed into *Escherichia coli* electrocompetent TG-1 cells (Cat. no. 60502-1, Lucigen, Middleton, WI). The two cloned repertoires, one from each llama, were submitted to two distinct sets of panning in which rIL-13 was coated on wells of microtiter plates at pH 8.2 or 9.3. The cloned Nbs were displayed on phage after rescue with M13KO7 helper phages to select the rIL-13−specific Nbs. Colonies were randomly selected after rounds 2, 3, and 4 and analyzed by ELISA on the periplasmic extract for the presence of Ag-specific Nbs. Anti−rIL-13−specific Nbs were sequenced and grouped in families according to their CDR3. Generation of the Nbs was delegated to the Flemish Institute for Biotechnology (VIB) Nanobody Core (Brussels, Belgium). The steps involving animals were approved by the ethical committees of the VIB Nanobody Core animal facilities under the protocol 13-601-1 "Eliciting an antigen-specific immune response in llamas or alpacas by immunization, aiming to select specific nanobodies for different antigens." All the manipulations made on the llamas followed all the regulations on animal welfare that apply in Belgium, which themselves are based on the European guidelines (Directive 2010/63/EU) for animal research.

Nb sequence reformatting

Formatting of Nbs carrying irregularities in their sequence or multivalent constructs was entrusted to GenScript (Leiden, the Netherlands). Multivalent or multiparatopic constructs were connected head to tail by a linker composed of a four-glycine motif followed by a serine, repeated seven times (G₄S)₇. Genes were cloned into pHEN6 expression vector, encoding a hexahistidine fused at the C terminus of the recombinant protein (57).

Expression and purification of rIL-13−specific Nbs

The specific anti−rIL-13 Nbs were produced as previously described in this study (56). Briefly, Nbs were expressed in *E. coli* WK-6 (58) cells using pMECS or pHEN6 vectors with Nbs overexpression induced by 1 mM isopropyl β-D-1-thiogalactopyranoside (Cat. No. I1401, Duchefa Biochemie, Haarlem, the Netherlands). Nbs were then extracted from the periplasm by osmotic shock and purified by two successive chromatography steps. First, samples were applied onto a Ni-NTA resin (Cat. no. 88222, Thermo Fisher Scientific, Waltham, MA) and eluted with PBS (pH 7.4) containing 0.5 M imidazole (Cat. no. 56750, Sigma-Aldrich, Overijse, Belgium). Fractions with absorbance at 280 nm above 0.2 were pooled and further purified by size-exclusion chromatography (SEC) using a HiLoad S75 16/600 column (Cat. no. 28989333, GE Life Sciences, Machelen, Belgium) and sterile PBS (pH 7.4) as eluent. Fractions containing proteins eluting either with an m.w. of 13,000−17,000 corresponding to Nb monomers or 26,000−30,000 for Nb dimers were pooled and concentrated on Vivaspin 2 (m.w. cutoff 3000; Cat. no. VS0291, Sartorius, Gottingen, Germany).

Expression and purification of rIL-13−specific Nbs in *Pichia pastoris*

The expression and purification of Nbs in yeast were conducted as described by Schoonooghe et al. (59). Briefly, the Nb genes were amplified by PCR, digested with SpeI and EcoRV restriction enzymes, and ligated into the corresponding sites of pAOXZalfa (S)HC yeast expression plasmids. Then, electrocompetent *P. pastoris* cells were transformed, seeded on agar plates, and incubated for 3−4 d. From these, 22 clones were selected and grown into a 24−deep well plate to assess the productivity of each clone. Protein expression was induced by adding 50 μl water:methanol (50:50 v/v) solution to each well. The protein expression of each clone was then assessed by a SDS-PAGE with Coomassie blue staining. The best-producing clone was chosen and stored at −20°C for subsequent productions. A 6-L scale production was then performed according to the same protocol as the expression studies, with all volumes scaled up accordingly. The product was successively purified by affinity chromatography using a Ni²⁺-loaded Chelating Sepharose Fast Flow column (GE Life Sciences) and eluted with a 20-mM phosphate buffer containing 0.4 M imidazole. SEC was used as a polishing method using a Superdex 200 C26 column (GE Life Sciences). Those productions were assigned to the Protein Service Facility of VIB (Ghent, Belgium).

Protein mass spectrometry

m.w. analyses were performed using a 1200 series rapid resolution liquid chromatograph coupled to a 6520 series electrospray ionization quadrupole time of flight (Q-TOF) high-resolution mass spectrometer from Agilent Technologies (Waldbronn, Germany). Compound separation was performed using a "BioResolve RP mAb polyphenyl, 450 Å, 2.7 μm particle size, 2.1 × 50 mm" column (Cat. no. 186008944, Waters, Milford, MA). Then, 1 μg

Nb was injected for each sample. The column temperature was set at 80°C. The mobile phases used in all experiments were composed of 0.08% formic acid + 0.02% trifluoroacetic acid in ultrapure water (solvent A) and 0.08% formic acid + 0.02 trifluoroacetic acid in acetonitrile (solvent B). The flow was settled at 0.5 ml/min. The applied gradient was as follows: 0 min, 15% solvent B; 0–10 min, 15–55% solvent B; 10–10.3 min, 55–80% solvent B; 10.3–11.3 min, 80% solvent B; 11.3–11.6 min, 80–15% solvent B; and 11.6–17 min, 15% solvent B. The column was conditioned according to the manufacturer's instructions. Electrospray Q-TOF parameters were as follows for simple mass spectrometer analysis: positive mode, 4 GHz resolution, mass spectrometer scan range 100–3200 mass–charge ratio (m/z) at 1 spectra/s, drying gas temperature 350°C, drying gas flow 10 L/min, nebulizer pressure 45 psi, capillary voltage 4500 V, Fragmentor 200 V, and Skimmer 65 V. Nitrogen was used as nebulizer gas. Continuous infusion of two reference ions, respectively, m/z of 121.050873 and 922.009798, was performed for Q-TOF calibration. Data acquisition and analysis were carried out by MassHunter Acquisition software for Q-TOF (Version B.04 SP3) and MassHunter Qualitative Analysis (Version B.07) software (both from Agilent Technologies). BioConfirm optional software (Version B.07) of MassHunter Qualitative Analysis was used for data analysis and m/z deconvolution.

Nbs affinity and specificity evaluation by ELISA

Nunc MaxiSorp microtiter plates (Cat. No. 44-2404-21, Thermo Fisher Scientific) were coated overnight at 4°C with 0.1 μg human rIL-13 per well in 100 mM carbonate buffer (pH 8.2) (Cat. no. 27775.293, VWR, Oud-Heverlee, Belgium). Free remaining protein binding sites were then blocked by adding 200 μL of a 1% (w/v) BSA (Cat. no. 37525, Thermo Fisher Scientific) solution and incubation for 2 h at room temperature. Meanwhile, samples were serially diluted in PBS supplemented with 0.05% (v/v) Tween 20 (PBST; Cat. no. P1754, Sigma-Aldrich). The diluted samples were added to the wells, and the plate was incubated for 1 h at room temperature and shaken at 200 rpm. Then, 100 μl/well of a 10,000 times diluted rabbit anti-Nb polyclonal Ab conjugated to HRP (Cat. no. A01861, GenScript) was added and incubated for 1 h. The plate was washed two times with 400 μl/well of PBST (0.1% v/v) between each step. Finally, 100 μl/well of 3,3',5,5'-tetramethylbenzidine (Cat. no. 34028, Thermo Fisher Scientific) was added for 2 min, and the reaction was stopped with the same volume of 3 N orthophosphoric acid (Cat. no. 20624.295P, VWR, Leuven, Belgium). The absorbance in each well was recorded using a Multiskan FC plate reader (Thermo Fisher Scientific) at 450 nm (signal) and 570 nm (reference). Alternatively, instead of the human rIL-13, a natural variant of human rIL-13 (IL-13R130Q) (Cat. no. CYT-682, ProSpec, Rehovot, Israel) associated with asthma, a human rIL-13 biotinylated in vitro using the AviTag technology (Cat. no. IL3-H82E5, ACROBiosystems, Newark, DE), a rhesus macaque rIL-13 (Cat. no. 2674-RM-025/CF, R&D Systems, Minneapolis, MN), a murine rIL-13 (Cat. no. Z03191-50, GenScript), and a human rIL-4 (Cat. no. Z02925-50, GenScript) were used for coating to assess the specificity of the Nbs. The K_Ds were determined for each sample using Prism 7 software (GraphPad Software, San Diego, CA) through a nonlinear regression.

Competition assays between monomeric Nbs

To assess the binding competition of Nbs on rIL-13, basically the same protocol as described for the Nbs affinity estimation was used with the following adaptations. Serial dilutions of the first Nb (expressed from pHEN6 lacking a hemagglutinin tag) were made in PBST (0.05% v/v), and an equivalent volume of solution containing the second Nb fused with a hemagglutinin tag as expressed from pMECS vector (competitor) at a constant concentration (2-fold above its saturation concentration) was added to each dilution. A rabbit antihemagglutinin tag polyclonal Ab conjugated to HRP (Cat. no. PA1-29751, Thermo Fisher Scientific; dilution 1:10,000) was used to detect the amount hemagglutinin-tagged Nb bound to the coated rIL-13. The binding curves were generated using Prism 7 software through a nonlinear regression.

Competition assays between Nbs and rIL-13 receptors

The method was adapted from Ultsch et al. (60). Nunc MaxiSorp microtiter plates were coated overnight at 4°C with 1 μg per well of an anti–rIL-13R$_{\alpha 1}$ Ab (Cat. no. MAB146, R&D Systems). The remaining free protein binding sites were then blocked with 200 μl of a 1% (w/v) BSA solution for 2 h at room temperature. After blocking, 0.25 μg of rIL-13R$_{\alpha 1}$ (Cat. no. IL1-H5224, ACROBiosystems) was added to each well and incubated for 2 h. Meanwhile, serial dilutions of the Nb samples were made in PBST (0.05% v/v), and an equivolume of 80 nM biotinylated human rIL-13 in PBS (0.05% v/v) was added to each dilution. After 30 min of preincubation, 100 μl of the resulting solutions were pipetted into the wells, and the plate was further incubated for 1 h at room temperature under agitation (200 rpm). Next, 100 μl of a 10,000-fold diluted streptavidin–HRP conjugate (Cat. no.

N504, Thermo Fisher Scientific) was added to the wells to detect the biotinylated rIL-13 bound to the receptor. Between each step, the wells were washed two times with 400 μl PBST (0.1% v/v). Finally, 100 μl/well of 3,3',5,5'-tetramethylbenzidine was added to each well for 2 min. The reaction was stopped with 100 μl/well of 3 N orthophosphoric acid. The absorbance in wells was read with the Multiskan FC plate reader at 450 nm (signal) and 570 nm (reference). The binding curves were generated with Prism 7 software through a nonlinear regression.

Human embryonic kidney–Blue human rIL-4/rIL-13 cell–based reporter assay

Usually, the TF-1 cell line is the gold standard to evaluate IL-13 activity in vitro. However, because these cells were found to be sensitive to endotoxin contaminations and as most of the Nbs were produced in bacteria, we preferred human embryonic kidney (HEK)–Blue IL-4/IL-13 cells (InvivoGen, San Diego, CA) that are more tolerant to endotoxins. The HEK-Blue IL-4/IL-13 cells are HEK293 cells transfected with the human STAT6 gene and a STAT6-inducible secreted embryonic alkaline phosphatase reporter gene, which is secreted upon stimulation of IL-13 and IL-4 (61–64). These cells were cultured and maintained in DMEM with high glucose, GlutaMAX, and pyruvate (Cat. no. 11965092, Thermo Fisher Scientific), supplemented with 10% (v/v) FBS (Cat. no. 11965092, Thermo Fisher Scientific), 50 μg/ml streptomycin, 50 UI/ml penicillin (Cat. no. 15140122, Thermo Fisher Scientific), and 100 μg/ml normocin (Cat. no. ant-nr-1, InvivoGen). At passage 3, selection antibiotics Zeocin and blasticidin (Cat. no. ant-zn-05 and Cat. no. ant-bl-05, InvivoGen, respectively) were added to the medium at concentrations of 100 and 10 μg/ml, respectively. The cells were passaged every time the confluence reached 70–90%.

To evaluate the Nb-neutralizing potency, Nb samples were serially diluted seven times in culture medium without antibiotics. An equivolume of human rIL-13 (2 ng/ml = 4-fold its 75% effective concentration [EC$_{75}$]) was added to each dilution, and 50 μl of the mixtures were placed into the wells of a Nunc Edge 2.0 96-well plate (Cat. no. 167425, Thermo Fisher Scientific). The plate was placed for a minimum of 30 min at 37°C. Meanwhile, the cell suspension was adjusted to a concentration of $4–8 × 10^5$ cells/ml and seeded with 50 μl/well. The plate was finally incubated for 24 h at 37°C with a steady supply of 5% CO$_2$. Then, 20 μl of supernatant from each well was pipetted into the well of a new 96-well plate containing 200 μl of QuantiBLUE medium (Cat. no. rep-qb1, InvivoGen) and further incubated at 37°C for 2 h. Finally, the absorbance was recorded at 655 nm with the Multiskan FC plate reader. The results were normalized according to the response obtained by stimulation with rIL-13 (100%) and the response obtained when no rIL-13 was added onto the cells (0%). To assess the validity of the experiment, a negative control [Nb targeting the β-lactamase II from *Bacillus cereus* (57)] and a positive control (neutralizing anti–rIL-13 murine mAb; Cat. no. 32116, Thermo Fisher Scientific) were used in each experiment at a final concentration of 2 mg/ml (≈66.7 μM) and 5 μg/ml (≈66.7 nM), respectively. rIL-13–related cytokines (IL-13R130Q, biotinylated human rIL-13, *Macaca mulatta* rIL-13, murine rIL-13, and human rIL-4) were also assessed, with a final concentration equal to their EC$_{75}$. The data were analyzed using Prism 7 software, and inhibition curves were drawn using nonlinear regression.

Statistical analysis

Results are all expressed as the mean ± SEM.

Affinity. Variance of the samples were compared using the Brown–Forsythe test. When homoscedasticity was verified, one-way ANOVA was used to compare K_D after Log$_{10}$ transformation. In the case of statistical significance (p value < 0.05), Tukey multiple comparison test was used as a post hoc test. When homoscedasticity was not verified, a Kruskal–Wallis test was used on Log$_{10}$ (K_D). In the case of statistical significance (p value < 0.05), Dunn multiple comparison test was used as a post hoc test.

Inhibitory activity. Variances of the data were compared using the Brown–Forsythe test. When homoscedasticity was verified, a one-way ANOVA was used. In the case of statistical significance (p value < 0.01), Dunnett multiple comparison was used as a post hoc test to detect the starting inhibitory concentration of samples by comparing each concentration of the samples to the apical control taken as the reference. Tukey multiple comparison test was used as a post hoc test to compare the IC$_{50}$s of the samples together after Log$_{10}$ transformation. When homoscedasticity was not verified, a Kruskall–Wallis test was used on Log$_{10}$-transformed data. In the case of statistical significance (p value < 0.01), Dunn multiple comparison test was used as a post hoc test.

Competition studies. Variance of the data were compared using the F test. When homoscedasticity was verified, an unpaired t test was applied to compare the K_D of the two conditions after Log$_{10}$ transformation. When

homoscedasticity was not verified, a Mann–Whitney U test was applied (p value was set at 0.05 in both cases).

Results

The first objective was to generate various Nb that recognize IL-13 and to select the highest producers with the lowest IC_{50}s and K_Ds. By designing multimeric constructs from these Nbs, we aimed to enhance their in vitro biological activity and to demonstrate their specificity for human IL-13. Finally, by investigating how the Nb might prevent the association of IL-13 to one of its receptor subunits (IL-13Rα1), we hoped to reveal the mechanism of inhibition.

Selection of monomeric Nb leads

Generation and production of rIL-13–specific Nb. After a short immunization of two llamas with glycosylated rIL-13, we constructed two separate immune libraries of the Nbs from the lymphocyte cDNA. Two Nbs libraries were obtained: "Core 66" library with a size of $\sim5 \times 10^8$ independent transformants and "Core N" library with a size of $\sim10^9$ independent transformants. About 79% of transformants from Core 66 library and $\sim80\%$ of transformants from Core N library harbored the vector with the right insert size. A first set of panning was performed whereby the rIL-13 was coated to the well of microtiter plates at pH 8.2, which is below the isoelectric point of rIL-13 (pH 8.8), to limit protein denaturation and to maximize recognition of the native rIL-13 conformation. Although physiological pH (7.2 to 7.4) was first considered, it was too far from the isoelectric point of IL-13 and would have resulted in highly positively charged protein, interacting poorly with the positively charged plastic plates. Results of this panning yielded 20 different Nbs specific to rIL-13, with CDR3s that grouped into three different families. Then, a second set of panning was performed whereby the rIL-13 was coated onto the polystyrene in a solution of pH 9.3, well above the isoelectric point of the Ag, in an attempt to maximize adsorption and retrieve even low-affinity binders. From this second panning, a total of 18 Nbs were collected that belong to five different families. Two of these families (family 4 and 5) were absent in the first set of panning. Collectively, we obtained a total of 38 different Nbs recognizing human rIL-13. These were all from the same llama, which was immunized with a higher dose of rIL-13, and were categorized in five different families (Table I). Among those Nbs, 2ILT86 (Nb family 2) and 2IL172 (the sole representative of family 4) carried mutations in their framework 4 sequence that were corrected to the consensus framework 4 sequence (a deletion of 1 aa occurred, possibly resulting from an artifact during the cloning/ligation during the library construction).

Out of the 38 Nbs, 29 were successively produced and purified by immobilized metal affinity chromatography and SEC in good yields (Table II). Among the nine Nbs that produced poorly, 2IL66 was the only representative of family 5, and thus, this Nb was recloned in *P. pastoris* in which excellent expression levels were

obtained (Table II). Once produced, the Nbs were analyzed by mass spectrometry to ensure that they matched the expected m.w., as calculated from their amino acid sequence. Except for one sample (4ILT41) that harbored an m.w. above the expected value, all samples matched their theoretical m.w., with differences below 75 ppm (≈1 for a protein of 15,000 such as Nbs; Table II). For most samples, the mass spectrum revealed a peak of significant intensity at 17 prior to the peak containing the correct theoretical m.w. This weight shift corresponds to a pyroglutamate derivative formed by cyclization of glutamine at the N terminus of the Nbs sequence (65).

Affinity of Nbs for rIL-13. The affinity of the Nbs for IL-13 was estimated by ELISA and varied strongly across the families (Table II). The best affinities were observed for Nbs of family 3 (K_D in the low-nanomolar range (2.3 ± 0.2 nM to 15 ± 6 nM). The Nbs from family 2 showed an acceptable affinity to human rIL-13 in the midnanomolar range (K_D of 52 ± 2 nM up to 150 ± 20 nM; Table II). The remaining Nbs from families 1, 4, and 5 showed low affinity for rIL-13 as none of them reached K_D values below 500 nM.

rIL-13 biological inhibition assay. Candidates from families 2 and 3, combining the best affinity for rIL-13 ($K_D < 100$ nM) and the best expression yield (> 1.0 mg/L), were selected for initial biological inhibition tests. Three candidates from family 2 (3ILT14, 3ILT82, and 4ILT14) and two candidates from family 3 (3ILT50 and 2IL43) were selected. Among family 3 members, 2IL43 was preferred over 3ILT58 because of its higher expression yields and despite its slightly lower affinity. Moreover, despite a low affinity ($K_D > 1$ μM), Nbs from family 1 (4ILT84 and 2IL134), family 4 (2IL172), and family 5 (2IL66) were also included to reveal a possible correlation between affinity and biological inhibition.

Nbs from families 2, 3, and 4 showed a statistically significant inhibition of the biological activity of human rIL-13 (ANOVA, $p < 0.01$; Fig. 1). Depending on the samples, the starting inhibitory concentration was quite variable compared with the apical control (where no Nb was added), even among the Nbs belonging to the same family. For family 2 Nbs (Fig. 1B), 3ILT82 showed a statistically significant inhibition starting from 3 μM (Dunnett multiple comparison test, $p < 0.01$), whereas 4ILT14 begun to inhibit rIL-13 activity only from 13 μM (Dunnett multiple comparison test, $p < 0.01$) and 3ILT14 from 12 μM (Dunnett multiple comparison test, $p < 0.01$). Despite showing a much higher affinity for the human rIL-13 than Nbs from family 2, Nbs from family 3 showed inhibitory potency within the same range (Fig. 1C): 2IL43 showed a significant inhibition of rIL-13 starting from 5 μM (Dunnett multiple comparison test, $p < 0.01$) and 3ILT50 from 12 μM (Dunnett multiple comparison test, $p < 0.01$). Finally, despite its very low affinity for human rIL-13 ($>1-10$ μM), 2IL172 from CDR3 family 4 significantly inhibited the biological activity of human rIL-13 starting from a Nb concentration of ~24 μM (Dunnett multiple comparison test; $p < 0.01$; Fig. 1D). No human rIL-13 inhibition was observed for Nbs

Table I. Sorting of the Nbs according to the sequence of their CDR3 family

Family According to CDR3 Sequence	Member(s)
Family 1	2ILT31, 2ILT90, *2ILT86*, 2ILT65, 3ILT69, 4ILT84, 2IL106, 2IL147, 2IL180, 3IL58, 3IL86, 2IL49, 2IL88, 2ILT23, 3IL73, 3ILT10, 4ILT63, 2IL159, 3IL37, 2IL50, 2IL134
Family 2	3ILT14, 4ILT14, 3IL78, 3ILT82, 4IL46, 2IL139, 4ILT83, 4ILT41, 4ILT86
Family 3	3ILT32, 3ILT50, 3ILT58, 2IL43, 3ILT64, 2IL61
Family 4	*2IL172*
Family 5	2IL66

Nbs were generated following the immunization of two llamas and their panning by phage display. Underlined Nbs carried a premature amber STOP codon (TAG), resulting in truncated Nbs in nonsuppressor bacteria strains. Nbs in italic and bold carried a sequence modification in their framework 4 that deviates from the consensus Nb sequences and may lead to nonfunctional Nbs.

Table II.   Properties of anti–IL-13 monomeric Nbs

Name	Nb Family	Theoretical m.w.	$\Delta_{m.w.}$ (ppm)	Expression Host (Vector)	Total Production Yield (mg/L)	K_D (nM)	IC_{50} (μM)
4ILT84	1	14961.3	20	*E. coli* (pMECS)	3.8	>500 nM	N.C.
2IL134	1	14949.3	62	*E. coli* (pMECS)	1.9	>500 nM	N.C.
3ILT14	2	15028.5	12	*E. coli* (pMECS)	1.0	70 ± 10	N.C.
3ILT82	2	15041.5	42	*E. coli* (pMECS)	2.9	52 ± 2	90 ± 10
4ILT14	2	15055.5	6	*E. coli* (pMECS)	2.5	96 ± 6	80 ± 20
4ILT83	2	15067.5	47	*E. coli* (pMECS)	1.3	150 ± 20	N.A.
3ILT32	3	15081.8	57	*E. coli* (pMECS)	0.5	15 ± 6	N.A.
3ILT50	3	15051.7	38	*E. coli* (pMECS)	1.7	2.3 ± 0.2	N.C.
3ILT58	3	14925.6	57	*E. coli* (pMECS)	1.1	4.3 ± 0.4	N.A.
2IL43	3	13611.8	0	*E. coli* (pHEN6)	1.2	6.0 ± 0.3	60 ± 10
2IL61	3	14994.7	25	*E. coli* (pMECS)	1.2	7 ± 1	N.A.
2IL172	4	13428.8	46	*E. coli* (pHEN6)	1.1	>500 nM	N.C.
2IL66	5	13515.8	30	*P. pastoris* (pAOXZalfa(S)HC)	50.6	>500 nM	N.C.

Properties of anti–IL-13 monomeric Nbs, including 1) the Nb family group, 2) the name of each Nb, 3) their theoretical m.w. based on their amino acid sequence, 4) the difference between the theoretical m.w. and the m.w. calculated from mass spectrometry analysis ($\Delta_{m.w.}$), 5) the expression system (plasmid vector), 6) the production yield after a double purification (immobilized metal affinity chromatography and SEC), 7) the K_D assessed via ELISA (mean ± SEM of minimum two independent experiments with three replicates each), and 8) the calculated IC_{50} based on extrapolated data (mean ± SEM of minimum two independent experiments with four replicates each).
    N.A., not applicable because activity was not assessed for these Nbs; N.C., not converged as the measured points did not allow extrapolation.

from families 1 (4ILT84 and 2IIL134; Fig. 1A) and 5 (2IL66; Fig. 1D) at the concentrations that were tested (ANOVA; $p > 0.01$; Fig. 1). The curves for samples with enough data points (2IL43, 4ILT14, and 3ILT82) were extrapolated using nonlinear regression, and the IC_{50} was calculated (Table II). No significant differences were observed between the IC_{50} of 2IL43, 4ILT14, and 3ILT82 (one-way ANOVA after $\log_{10}[IC_{50}]$ transformation, $p > 0.01$).
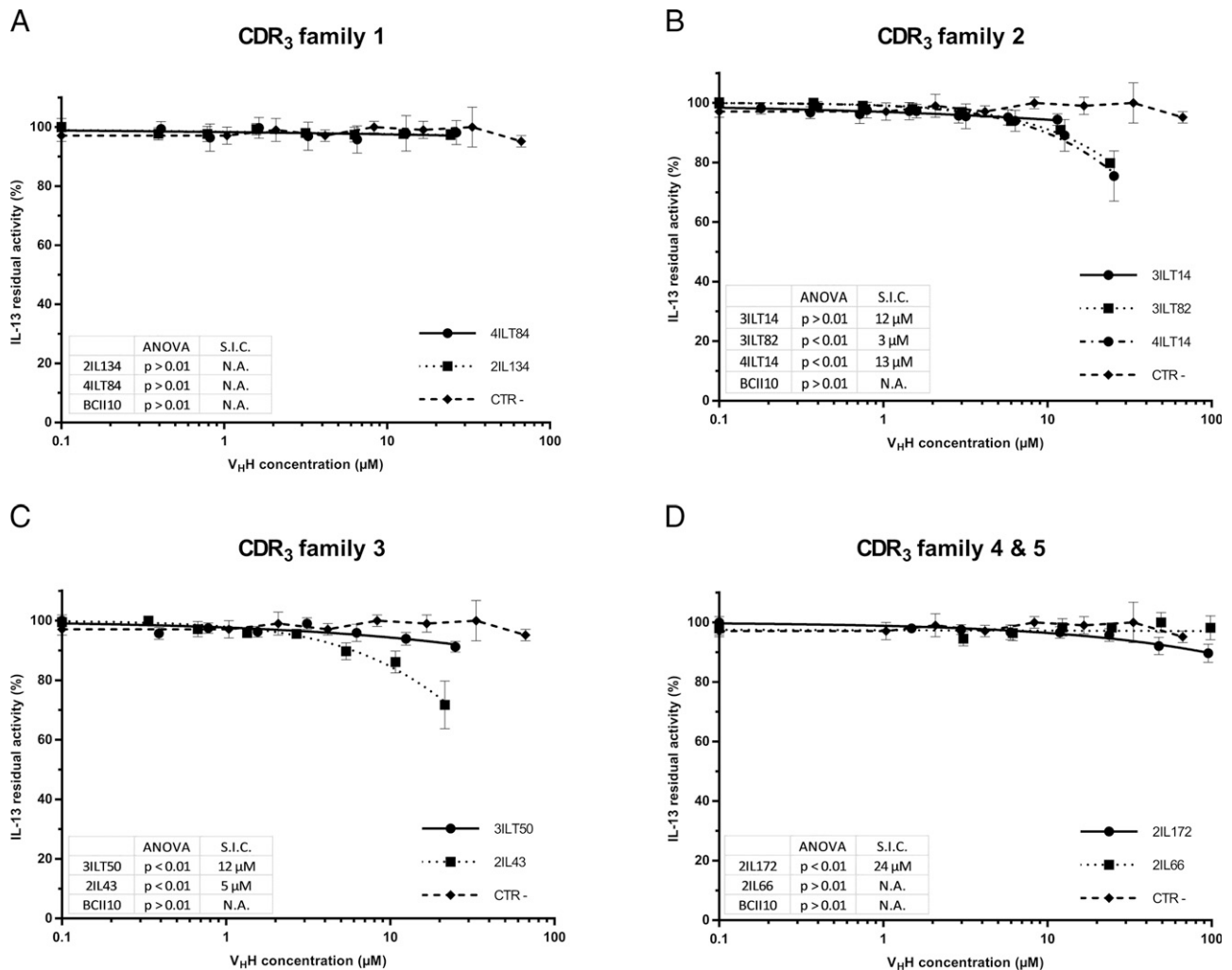

FIGURE 1.   Antagonist activity of the monomeric anti–rIL-13 Nbs for representative of (**A**) CDR3 family 1, (**B**) CDR3 family 2, (**C**) CDR3 family 3, and (**D**) CDR3 family 4 and 5. Dose-response curves generated during the in vitro potency assay based on engineered HEK cells responding specifically to rIL-13 or human rIL-4. The curves are compared with the negative control (CTR⁻) anti-β-lactamase-II-10 Nb. Statistical analysis was performed with an ANOVA test and, when appropriate, with Dunnett test taking the apical control (extreme-left value, 100%) as the reference group. The p value was set at 0.01. Results are expressed as the mean ± SEM obtained from a minimum two independent experiments, each including minimum four to eight replicates. S.I.C., starting inhibitory concentration.

Dimer design and selection

Production of rIL-13–specific dimeric Nb constructs. Despite the observation of a weak inhibition of the biological activity of rIL-13, the required Nb doses were several decades higher than those that were reported in the literature for anti–rIL-13 mAbs entering clinical trials (16, 66–68). Those Nb concentrations seemed to be unrealistic to be delivered to patients. Consequently, designing multimeric constructs made from the best Nbs was envisaged to increase the avidity and concomitantly the likelihood of sterically interfering with the IL-13/IL-13R interaction. The Nbs that showed the lowest starting inhibitory concentration in the inhibition assay using HEK-Blue IL-4/IL-13 cells that belonged to families 2 and 3 (3ILT82 and 2IL43; Fig. 1B, 1C). These were selected and formatted into multivalent and multiparatopic constructs. First, a competition study between the two monomers (3ILT82 and 2IL43) was performed to ensure that these Nbs do not compete for the same epitope on rIL-13. For this study, the binding curves of 3ILT82, alone and in the presence of a saturated concentration of 2IL43, were assessed, and K_Ds were determined from both conditions. There was no statistically significant difference between the K_Ds of 3ILT82 alone and of 3ILT82 in the presence of 2IL43 (52 ± 2 and 70 ± 10 nM, respectively; *t* test after $\log_{10}$ [K_D] transformation, *p* > 0.05).

The Nb subunits were connected to each other through a G_4S linker motif, which ensures a good flexibility and solubility. In the absence of information about the distance of the Nb epitopes on rIL-13, it was decided to repeat the motif 7-fold to guarantee sufficient spacing between the different Nb subunits so that both entities could bind simultaneously to their respective epitopes.

Bivalent (3ILT82$_{biv.}$ and 2IL43$_{biv}$) and biparatopic (2IL43/3ILT82 and 3ILT82/2IL43) constructs were generated (Fig. 2).

Different expression yields for the bivalent constructs were noted, which were dependent on the dimer and on the expression level of the composing monomers (Tables II and III). Unlike monomers, in which only one main peak (area under the curve between 80 and 95%) was consistently present in their SEC chromatograms, some of the dimeric constructs showed main peak shouldering or even multiple peaks of the same intensities (3ILT82/2IL43 and 2IL43$_{biv.}$, respectively; data not shown). In cases in which several peaks within the chromatogram occurred, the two closest from the theoretical elution time of dimeric Nbs were harvested and further differentiated by mass spectrometry. Mass spectrometry analysis showed that the best producer (3ILT82$_{biv.}$) contained only the correct species and a moderate proportion of the pyroglutamate derivative species, whereas the worst producer (2IL43$_{biv.}$) was highly degraded, with no species corresponding to the theoretical m.w. of the Nb dimer (Table III). Apart from the pyroglutamate derivative species, the biparatopic Nbs contained a few other peaks (intensity of 3–4%) corresponding to a lower m.w. than expected (Table III) but with sufficiently close m.w. to coelute with the main species during the purification step by SEC (>20,000). No further action was taken in terms of purification, and samples were used as such for further studies.

Binding effects of multivalent and multiparatope constructs. The dose-response binding curves of bivalent Nbs from ELISA were used to estimate the K_Ds (Table III). The affinity of the bivalent construct (3ILT82$_{biv.}$) for rIL-13 improved considerably (K_D = 1.4 ± 0.1 nM) compared with its monomeric subunit (3ILT82, K_D = 52 ± 2 nM) (Tukey multiple comparison test after $\log_{10}$ [K_D] transformation, *p* < 0.05). The heterodimers comprising 3ILT82 and 2IL43 subunits also showed a significant affinity
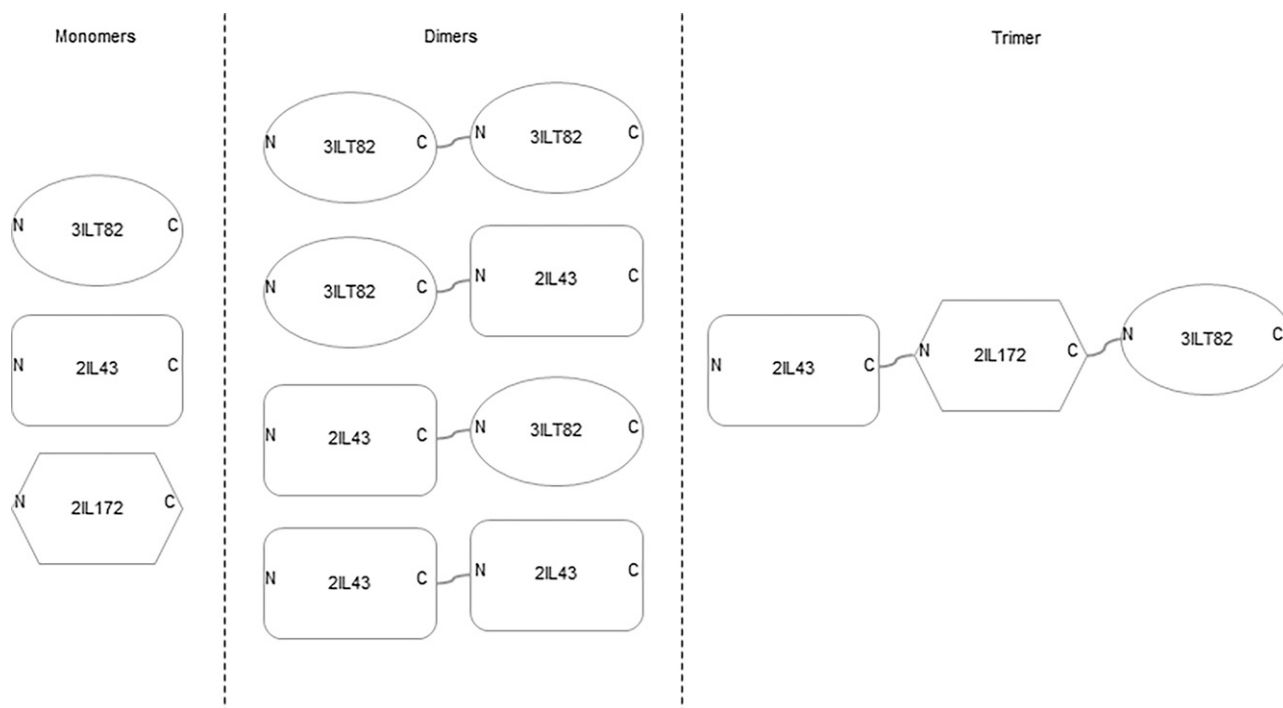

FIGURE 2. Schematic representation of constructs that were designed for this study. Oval shape represents the monomeric Nb 3ILT82 (CDR family 2), rectangle shape represents the monomeric Nb 2IL43 (CDR family 3), and diamond shape represents the monomeric Nb 2IL172 (CDR family 4). Monomeric subunits were assembled to form bivalent (3ILT82$_{biv.}$ and 2IL43$_{biv.}$) and biparatopic (3ILT82/2IL43 and 2IL43/3ILT82) dimeric constructs. A triparatopic construct was also assembled from three different monomeric Nbs. Each of the monomeric subunits were linked together using a synthetic linker composed of a 7-fold repeated motif of four glycine and one serine [(G4S)₇], represented by the s-shaped line. N terminus and C terminus side of each monomer are represented by the N and C letters, respectively, to show the order in which the monomeric constructs were assembled.

Table III.   Anti-IL-13 multimeric Nbs properties

Name	Nb Family	m.w. (ppm)	Correct/PyrogGlu/Other	Expression Host (Vector)	Expression Yield (mg/L)	K_D (nM)	IC_{50} (μM)
3ILT82biv.	2/2	28708 (27)	71%/29%/0%	*E. coli* (pHEN6)	3.6	1.4 ± 0.1	28 ± 2
2IL43biv.	3/3	28592 (N.A.)	0%/0%/100%	*E. coli* (pHEN6)	N.A.	N.A.	N.A.
3ILT82/2IL43	2/3	28650 (28)	78%/19%/3%	*E. coli* (pHEN6)	0.5	2.6 ± 0.2	0.73 ± 0.04
2IL43/3ILT82	3/2	28650 (20)	76%/20%/4%	*E. coli* (pHEN6)	0.9	2.8 ± 0.3	0.60 ± 0.03
2IL43/2IL172/ 3ILT82	3/2/4	43445 (15)	72%/0%/28%	*P. pastoris* (pAOXZalfa(S)HC)	10.0	1.60 ± 0.04	0.20 ± 0.01

Anti-IL-13 multimeric Nbs properties, including 1) the name of each Nb, 2) the Nb family, 3) the m.w. calculated from mass spectrometry analysis (difference between the theoretical and the measured m.w.), 4) the relative amount of each subtype of peak detected by mass spectrometry, 5) the expression system (plasmid vector), 6) the production yield after a double-step purification (immobilized metal affinity chromatography and SEC) in mg per liter of culture, 7) the K_D estimate from ELISA (results are expressed as mean ± SEM of minimum two independent experiments, each in triplicate), and 8) the inhibitory activity with its IC_{50} (results are expressed as mean ± SEM of minimum two independent experiments, with minimum four replicates each).

N.A., not applicable because activity was not assessed.

increase (K_Ds = 2.6 ± 0.2 nM and 2.8 ± 0.3 nM for 3ILT82/2IL43 and 2IL43/3ILT82, respectively). Because 2IL43 (K_D 6 ± 1 nM) had comparable high affinity for rIL-13, it is clear that the affinity gain upon dimerization is lower than that observed for 3ILT82biv. (Tukey multiple comparison test after Log_{10} [K_D] transformation, $p < 0.05$). The order in which the subunits within the heterodimer were assembled was irrelevant for the affinity enhancement (Tukey multiple comparison test after Log_{10} [K_D] transformation, $p > 0.05$).

As for the monomers, the multimer inhibitory activity was also evaluated for the dimer constructs, using the HEK-blue human IL-4/IL-13 cell line (Fig. 3). Despite the minor affinity enhancement for rIL-13, the biparatopic Nbs (3ILT82/2IL43 and 2IL43/3ILT82) yielded a highly improved inhibitory potency against rIL-13 (IC_{50}s = 0.73 ± 0.04 μM and 0.60 ± 0.03 μM, respectively) in comparison with either 3ILT82 or 2IL43 (IC_{50}s = 90 ± 10 μM and 60 ± 10 μM, respectively) (Tukey multiple comparison test after Log_{10} [IC_{50}] transformation, $p < 0.01$). Likewise to the affinity, the order in which the Nb subunits were assembled had no impact on their inhibitory

potency (Tukey multiple comparison test with Log_{10} [IC_{50}] transformation, $p > 0.01$). In contrast, despite a highly significant improvement in affinity compared with 3ILT82 (37-fold), 3ILT82biv. exhibited only a minor improvement in its inhibitory potency (IC_{50} = 28 μM ± 2 μM) relative to its monomeric subunit (3ILT82, IC_{50} = 90 μM ± 10 μM). Nevertheless, this minor difference was statistically significant (Tukey multiple comparison test after Log_{10} [IC_{50}] transformation, $p < 0.01$).

Evaluation of a triparatopic construct

In view of the success to improve the rIl-13 biological inhibitory activity with Nb heterodimers, we decided to construct a triparatopic Nb including 2IL172 (Fig. 2), which showed also a low inhibitory activity. Because the dimeric constructs (2IL43biv. and 3ILT82/2IL43) suffered from degradations when expressed in *E. coli*, the triparatopic construct (2IL43/2IL172/3ILT82) was produced in *P. pastoris*. The mass spectrometry analysis showed that the main species corresponded to the expected m.w., and almost no molecules with
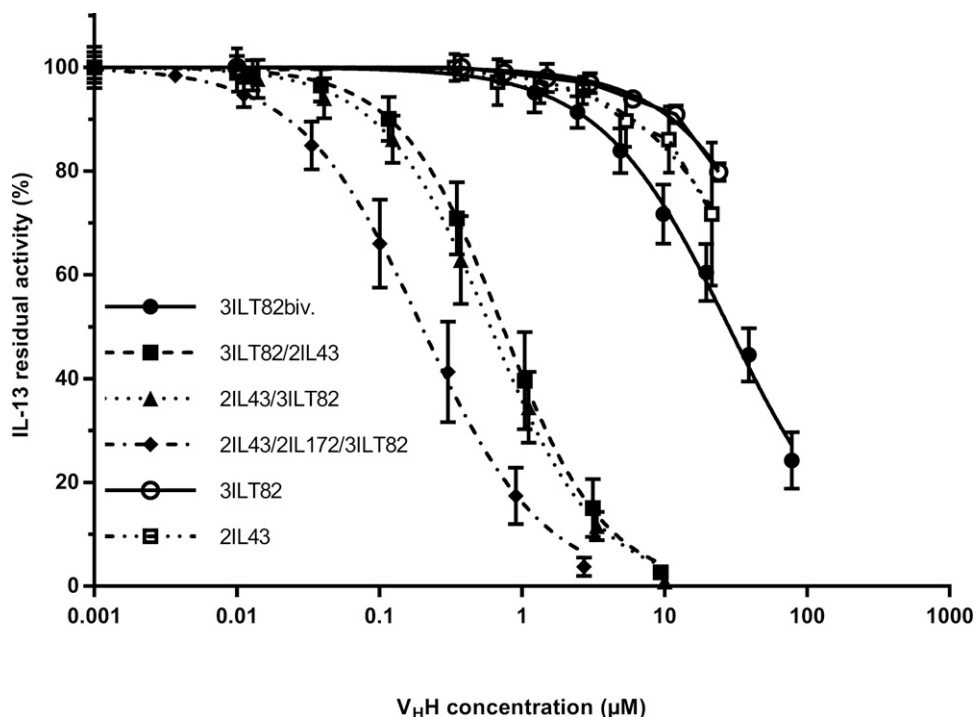

FIGURE 3.   Antagonist activity of the multimeric anti–rIL-13 Nbs. Dose-response curves generated during the in vitro potency assay based on engineered HEK cells, responding specifically to rIL-13 or human rIL-4. Statistical analysis was performed with an ANOVA test and, when appropriate, with Dunnett test taking the apical control (extreme-left value; 100%) as the reference group. The *p* value was set at 0.01. Results are expressed as the mean ± SEM of minimum two independent experiments, each including minimum four replicates, except for the positive control, which was done on only one experiment including four replicates because of the limited amount of material.

pyroglutamate were noticed (Table III). However, a repetitive pattern of a constant loss of weight (315) was observed for which no obvious explanation could be put forward. No further attempts were made to improve the purification of the sample, and it was used as such for further studies.

The K_D of the triparatopic Nb for rIL-13 was further lowered (K_D = 1.60 nM ± 0.04 nM) in comparison with the biparatopic construct (2.6 ± 0.2 nM and 2.8 ± 0.3 nM for 3ILT82/2IL43 and 2IL43/3ILT82, respectively), but the difference was not statistically significant (Tukey multiple comparison test after Log_{10} [K_D] transformation, $p > 0.05$). The biological inhibitory activity toward rIL-13 was further increased (IC_{50} = 200 ± 10 nM), although without statistically significant difference relative to the biparatopic dimers (IC_{50}s = 730 ± 40 nM and 600 ± 30 nM for 3ILT82/2IL43 and 2IL43/3ILT82, respectively; Tukey multiple comparison after Log_{10} [IC_{50}] transformation, $p > 0.01$). Overall, the triparatopic Nb construct exhibited a 300-fold inhibitory potency increase relative to the monomeric subunit displaying the lowest IC_{50} (IC_{50} = 0.20 ± 0.01 μM for 2IL43/2IL172/3ILT82 versus 60 μM ± 10 μM for 2IL43).

For further characterization, this triparatopic construct (2IL43/2IL172/3ILT82) was preferred over the biparatopic constructs for further characterization because it showed a good production yield in yeast as well as a better stability regarding thermal denaturation and aggregation (data not shown). Moreover, despite nonstatistically significant differences with the dimers, both its K_D and IC_{50} were the lowest.

Binding specificity of the triparatopic construct for human rIL-13. The other proteins that were related to it were also tested, and an ELISA was used to evaluate the ability of 2IL43/2IL172/3ILT82 to associate with various IL-13 molecules (Fig. 4). Apart from the human rIL-13 Ag, 2IL43/2IL172/3ILT82 was able to bind IL-13R130Q, which differs by one single amino acid [>99% similarity (1)], with the same affinity (K_D = 1.3 ± 0.1 nM) and for which no statistically significant difference was observed (Tukey multiple comparison test after Log_{10} [K_D] transformation, $p > 0.05$). Likewise, 2IL43/2IL172/3ILT82 was also able to associate with the *Macaca mulatta* rIL-13 [95% similarity, UNIPROT database (1)], except that for this derivative, the affinity was even better (K_D = 0.36 ± 0.02 nM) than for human rIL-13 (K_D = 1.60 ± 0.04 nM), and the difference was statistically significant (Tukey multiple comparison test after Log_{10} [K_D] transformation, $p < 0.05$). Conversely, the triparatopic construct was unable to recognize the least-related variants, such as murine rIL-13 [56.8% similarity, UNIPROT database (1)] and human rIL-4 [20–25% similarity (2)].

The inhibitory potency of 2IL43/2IL172/3ILT82 toward the proteins related to its cognate Ag was also assessed in the cell-based assay involving the engineered HEK cells (Fig. 4). The inhibition results for IL-13R130Q mutant with IC_{50} = 330 ± 30 nM versus 200 ± 20 nM for rIL-13, and a nonstatistically significant difference (Tukey multiple comparison test after Log_{10} [IC_{50}] transformation, $p > 0.01$) correlated well with the binding efficiencies. As expected from the lack of association between the triparatopic Nb construct and murine rIL-13 or human rIL-4, the 2IL43/2IL172/3ILT82 was unable to inhibit the in vitro biological activity of these IL-13–related proteins. Conversely, 2IL43/2IL172/3ILT82 failed to inhibit the in vitro activity of *M. mulatta* rIL-13 at any concentration tested (ANOVA, p value > 0.01), despite its enhanced affinity for this human IL-13–related cytokine.

Competition studies between the triparatopic Nb and rIL-13R$_{\alpha 1}$. To further determine the mechanism of inhibition of the trimer, a competition study between rIL-13R$_{\alpha 1}$ and 2IL43/2IL172/3ILT82 for a biotinylated IL-13 was performed.

First, the affinity of 2IL43/2IL172/3ILT82 for the in vitro biotinylated rIL-13 was assessed (Fig. 4). The construct showed a significantly stronger affinity to the biotinylated Ag form than toward the human rIL-13 (K_D of 0.52 ± 0.02 nM versus 1.60 ± 0.04 nM, respectively; Tukey multiple comparison test after Log_{10} [K_D] transformation, $p < 0.05$). Despite its stronger affinity for the biotinylated rIL-13, the triparatopic construct was only able to prevent the formation of the primary complex "biotinylated rIL-13–IL-13R$_{\alpha 1}$" (Dunnett multiple comparison test after Log_{10} [IC_{50}] transformation; p value < 0.01) during the competition assay, with an estimated IC_{50} of 0.9 ± 0.2 μM (Fig. 5). The results were then confirmed on HEK-Blue IL-4/IL-13 cells, in which 2IL43/2IL172/3ILT82 was also able to inhibit the biological effect of the biotinylated rIL-13, starting from a concentration of 1.7 μM (Dunnett multiple comparison test after Log_{10} [IC_{50}] transformation, p value < 0.01; Fig. 4).

Discussion

The purpose of this study was to generate the basis of a new tool (based on Nbs) to treat IL-13–related disease, with a particular focus on asthma. The choice of Nbs was initially driven by their well-known enhanced stability and solubility that open up the possibility of considering other routes of administration than injection, such as the pulmonary route.

In this study, two biparatopic and one triparatopic Nb were designed from three Nb monomers with low activity (IC_{50} > 60 μM), resulting in 80–300-fold activity improvement in comparison with the most active monomeric subunit (2IL43). These findings are consistent with previous reports. They confirm that Nbs can be easily assembled in multivalent (54, 69–71) or multiparatopic (72) constructs from monomeric Nb subunits by using recombinant DNA technology, which can lead to a much more potent activity compared with the autonomous monomers. However, it is unlikely that the increase in activity in going from the monomeric subunits to the multiparatopic constructs should be attributed exclusively to the enhanced affinity (2–4 fold). Several hypotheses could explain this improvement in inhibitory activity. A first hypothesis would assume that the epitopes of 3ILT82 and/or of 2IL43 are at least partially overlapping with the binding site(s) of IL-13 to its receptor but without mutual overlapping (as demonstrated through the competition assay between both monomeric Nbs). As a result, combining the two subunits in one molecule may therefore have increased the surface shielded by the multiparatopic Nb constructs, thereby enhancing the steric hindrance between IL-13 and its receptor. Another hypothesis would favor a side chain rearrangement in the region close to the receptor binding site upon association with Nbs, which compromises the IL-13 recognition by its receptor. A third hypothesis might be a combination of the two previous ones. In any cases, using a unique construct binding two different epitopes has likely further strengthened their inhibitory capacity as the binding of one subunit increases the probability for the other subunit(s) to bind to the same IL-13 molecule, especially when low Ag concentrations in solution are used (cell-based assay: 0.5 ng/ml of IL-13 ≈ 40 pM). The partial binding overlap of each subunit with the IL-13 binding site(s) to the receptor might also explain why they both inhibit rIL-13 biological activity only in the micromolar range (IC_{50}s between 60 and 90 μM), despite a low-to-mid nanomolar affinity. In contrast, despite an apparent high improvement for its affinity toward rIL-13, 3ILT82$_{\text{biv.}}$ (K_D was reduced 37-fold) did not see its activity improved as much in vitro (4-fold). IL-13 is a soluble monomeric protein with no redundancy in its sequence. Hence, the functional affinity of 3ILT82$_{\text{biv.}}$, whose subunits bind to the same epitope, has been artificially increased in the ELISA as it uses adsorption of Ag on a solid surface, thereby increasing the local concentration of rIL-
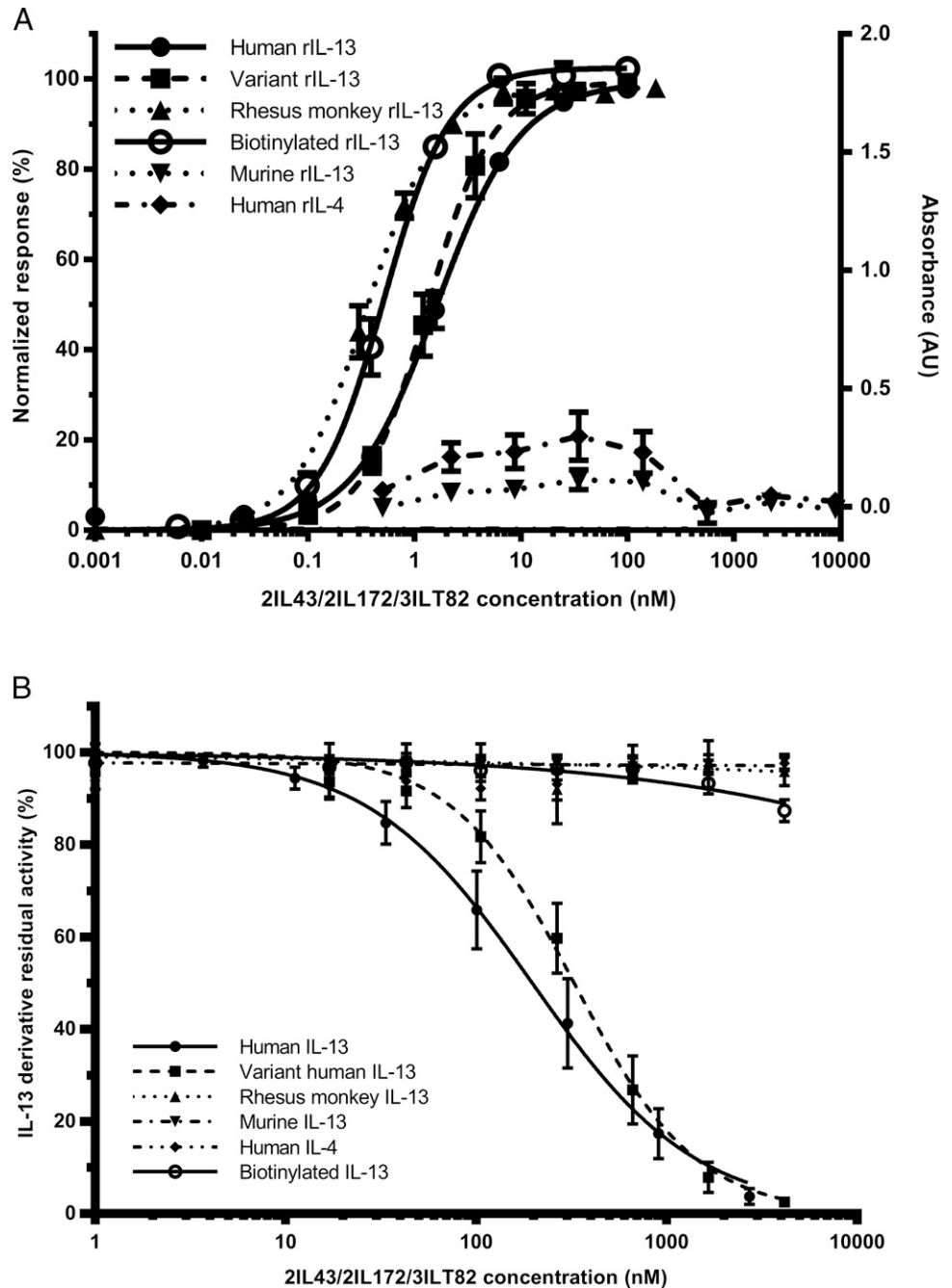
FIGURE 4. Specificity of the triparatopic Nb construct toward homologous rIL-13 variants. (**A**) The specificity of the triparatopic construct was investigated by ELISA on immobilized related Ag with increasing 2IL43/2IL172/3ILT82 concentrations. Results are expressed as the mean ± SEM of minimum two independent experiments, each including three replicates. (**B**) Specificity related to the inhibitory potency of the triparatopic Nb construct toward human rIL-13 and its homologous variants. Results are expressed as the mean ± SEM of minimum two independent experiments, each including four to eight replicates.

13. In the cell-based assay, rIL-13 is in solution at low concentration ($\approx$40 pM), and 3ILT82$_{biv.}$ did not benefit from the same avidity effect as in the ELISA.

Regarding the triparatopic Nb, adding the subunit 2IL172 further lowered the IC$_{50}$, but the difference was not statistically significant, probably because of the very low activity detected for the autonomous 2IL172 subunit. The reason for the small increase in the activity may be due either to the weak binding of 2IL172 to a third epitope or may simply be due to an additional steric hindrance effect because of the increased m.w. of the construct. The mechanism of IL-13 inhibition by the triparatopic construct was further investigated by a competitive ELISA and was partially explained by the prevention of IL-13 binding to its subunit receptor IL-13Rα1. It is still possible that at least one of the monomeric subunits prevents the binding of IL-4R on IL-13. In contrast, although IL-13Rα2 have been described to lead to some functional activity (10, 11), there is

no evidence currently available to support any role of IL-13Rα2 in asthma physiopathology. Therefore, we did not assess the competition of the constructs over IL-13Rα2.

The triparatopic construct, and therefore its subunits, also showed a high specificity regarding human IL-13, binding closely related proteins whose sequence similarity was $\geq$95% (UNIPROT database), including a nonnatural variant of IL-13, which was biotinylated through the AviTag technology. Those results were confirmed in the cell-based assay for the natural variant of IL-13R130Q, whose overexpression is often associated with asthma (73), but not for the *M. mulatta* rIL-13 or the biotinylated rIL-13. The fact that our construct binds better to both the *M. mulatta* rIL-13 and the biotinylated rIL-13 than to its native Ag but provided a weaker inhibition for the first two in the cell-based assay is difficult to explain without further investigation. One assumption might surmise that those two IL-13 derivatives were not as active as the native rIL-13 on HEK-Blue IL-

FIGURE 5. rIL-13 receptors subunit competitions experiment. The ability for the triparatopic construct 2IL43/2IL172/3ILT82 to outcompete rIL-13Rα1 for a biotinylated rIL-13. The competition was performed with immobilized receptor and a constant concentration of preincubated biotinylated rIL-13 with increasing concentrations of 2IL43/2IL172/3ILT82 (black curve) or of the positive control (CTR$^+$) anti−rIL-13 mAb validated to neutralize the in vitro activity of rIL-13 (green curve). An Nb (anti−β-lactamase-II-10) was also used as negative control (red curve). Results are expressed as mean ± SEM of two independent experiments performed in triplicate.
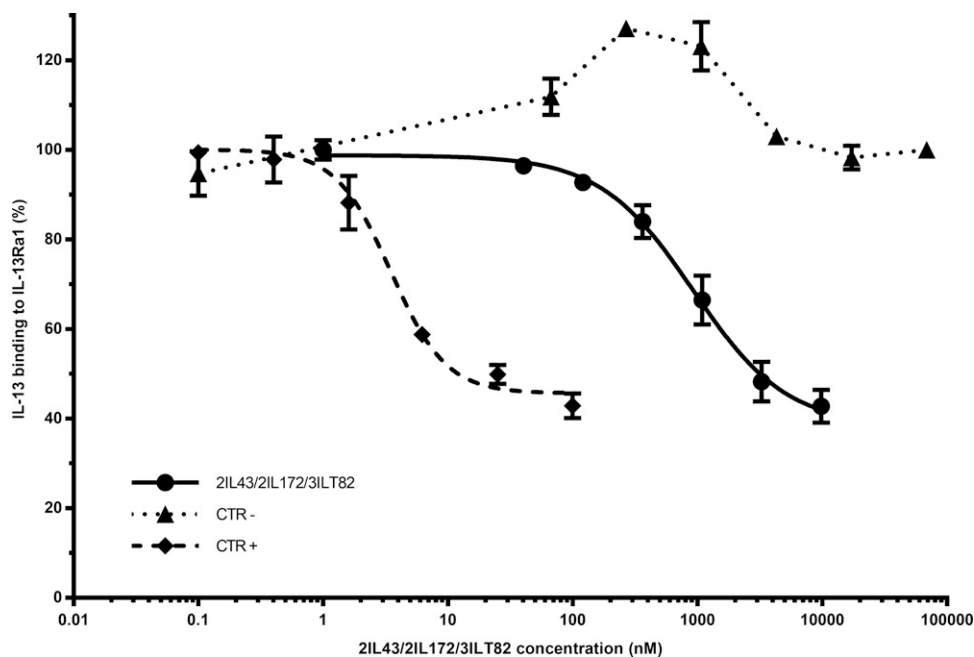
4/IL-13 cells; therefore, their concentrations in the test medium had to be increased to reach the EC$_{75}$ (7 ng/ml and 70 ng/ml, respectively, compared with 0.5 ng/ml for the human rIL-13 used as Ag). The increase in concentration might have impacted negatively the IC$_{50}$ of our triparatopic Nb construct. On the contrary, the triparatopic construct showed no affinity toward human IL-13−related proteins with lower similarity, such as a murine rIL-13 [57% similarity with human IL-13, UNIPROT database (1)] and human rIL-4 [20−25% similarity (2)] in the ELISA and the cell-based assay. Those two last results point to the high specificity of Nbs for their target and the unlikeliness to affect other pathways than IL-13 in vivo, thereby limiting possible side effects. However, it also raises concerns for future in vivo experiments, in which rodents are often the first choice of test subject. A possibility would be to administer human rIL-13 to mice, as Blanchard et al. (18) did to assess tralokinumab potency in mice because a cross-reactivity exists between the receptors and the IL-13 of both species.

Nbs of this study remain of lower activity than the anti−IL-13 mAbs that have been in clinical trials so far with IC$_{50}$ in the nanomolar range against picomolar range, respectively (16, 66−68). Nbs also have two main intrinsic properties that make their use or generation more complicated than for conventional Abs. Indeed, whereas Abs can be generated using multiple different (small) host animals, Nbs can only be generated by using Camelidae or sharks (for their counterpart, the new Ag receptor variable fragments "Vnar"). Their lower m.w. also renders their blood half-life very short, ∼30, 90, and 120 min for nonalbumin-binding monomeric, dimeric, and trimeric VHHs, respectively (74). Nonetheless, Nbs also possess massive advantages over complete mAbs, which counterbalance their lower activity and overcome the limitations of mAbs for asthma therapy.

First, bacteria (75) or yeast (76) are routine hosts to express properly folded Nbs, including the formation of disulfide bridges. These microbial expression systems significantly simplify the process development and drastically reduce the associated production costs over mammalian cells (77) as they require only inexpensive nutrition sources, have rapid growth (20-min doubling time for bacteria versus 1−2 d for mammalian cells), and achieve much higher cell densities (78).

Second, this study confirmed that anti-IL-13 Nbs, like Nbs targeting other Ags, can be engineered into multivalent or multiparatopic constructs. Actually, several Nbs that have entered clinical trials have been tested under a multivalent/paratopic/specific form (up to three units) to enhance either their activity (70, 79), their half-life (80), or both (81−83). Multivalency therefore does not seem to negatively impact their developability in terms of production and stability, although this may differ from molecule to molecule. To further improve the (monomeric, dimeric, or trimeric) constructs of this study, a Nb targeting another inflammatory mediator involved in moderate-to-severe asthma might be generated and combined to obtain a synergistic effect on the therapy. Similar strategies were already considered by big pharmaceutical companies with conventional Abs. Although the strategy considered was different, Sanofi and Regeneron proved with their dupilumab (Dupixent) that blocking IL-4 and IL-13 simultaneously by blocking IL-4R was more efficient than IL-13 monotherapy, succeeding where IL-13−exclusive therapy failed. IL-5 might also be a possibility as monotherapies targeting IL-5 were also successfully marketed, with mepolizumab (Nucala), reslizumab (Cinqaero), and benralizumab (Fasenra). Targeting T$_H$2 cytokines along with other cytokines might also be a strategy. T$_H$17 cytokines (i.e., IL-17 or IL-22) may broaden the efficacy to other poorly controlled types of asthma such as mixed neutrophilic−eosinophilic asthma in which T$_H$17 cytokines are suspected to be involved (84), and this strategy is already considered by Roche (85). Another promising target would be dual inhibition of IL-13 and thymic stromal lymphopoietin, for which Boehringer Ingelheim has already started to develop a bispecific Ab (86).

In contrast, assembling constructs with more than two units of Nbs together results in constructs with a size very similar to Fab, and one might think that the advantageous small size of Nbs is lost. Nonetheless, multimeric Nb constructs still conserve many advantages over Fab: 1) they still have enhanced stability because of their intrinsic characteristics; 2) at equal starting monomeric affinity with Fab, the multimeric construct of Nb may take advantage of their multivalency, which can lead to enhanced affinity or activity as it was shown in this study; and 3) the stability of multimeric constructs as they were designed in this study do not require interdisulfide bridges (even though they do possess intrachain disulfide

bridges). The use of multimeric constructs also has the advantage of increasing the half-life of the therapeutic over monomeric Nbs, which usually suffer from rapid clearance and thereby higher administration frequency. Combined with the strategy of local administration as well as a daily administration via a noninvasive pathway, Nbs therefore consist of a viable option compared with weekly injection for mAbs, which is invasive and inconvenient to patients.

Third, in the case of asthma, administration of the treatment is usually preferred by the pulmonary route. However, one of the limitations of mAbs is that they have a poor distribution to the lungs from the blood because of their poor diffusion/permeability through the membranes and their dilution within the whole organism. Indeed, studies have reported a ratio from ∼1:7 between the concentration of mAb in the lung compared with the concentration in serum (87). As mAbs used for anti–IL-13 therapy were administered by s.c. injection, the overall ratio of mAbs reaching their site of action is even lower. Currently, no mAbs are marketed for the pulmonary route. Only smaller and simpler proteins have already been successfully formulated for this route and approved by the U.S. Food and Drug Administration and/or the European Medicines Agency (i.e., insulin and DNase). Among potential future proteins investigated for inhalation, Nbs are particularly well suited given their small size, simple and robust structure, high thermal stability, and solubility (88). Recently, a proof of concept involving a trivalent Nb administered by nebulization was achieved to treat respiratory syncytial virus with a very low aggregation rate (<2%) (88). Considering the low distribution of mAbs to the lung, the difference of m.w. between complete conventional mAbs, and our heaviest Nb construct (trimeric is 3 times lighter than complete mAbs), Nbs administered directly to the lungs will, at equal IC_{50}s, require a dose at least 21-fold lower than the equivalent mAb dose administered by injection. In other words, if the same dose is delivered by both routes (pulmonary for Nb or injection for mAb), the Nb IC_{50} might be at least 21-fold higher than the mAb IC_{50} while resulting theoretically in the same efficacy.

Finally, with regard to the specific constructs generated during this study, several strategies might still be considered to further enhance the activity of the Nbs. One possible strategy would involve the improvement of the intrinsic affinity of one or several of the Nb subunits. Indeed, even if the increase in the apparent affinity of $3ILT82_{biv.}$ (because of avidity) did not increase the activity with the same magnitude, it remains possible that limited mutagenesis of the Nb paratope or its periphery would result in a concomitant improvement in the activity. Furthermore, independently of the multimeric forms that were designed, the K_D never reached subnanomolar values (lowest $K_D = 1.60 \pm 0.04$ nM for the triparatopic Nb), remaining in the same range of K_D of IL-13 for its subunit $IL13R_{\alpha 1}$ (2−10 nM) (3−6). As both K_Ds are within the same order of magnitude (except for the 3ILT82 subunit), both the Nb constructs and the $IL-13R_{\alpha 1}$ are expected to compete equally for IL-13. However, once IL-13 is bound to $IL-13R_{\alpha 1}$, the complex then recruits IL-4R, which further tightens the binding to a subnanomolar level (32-400 pM) (5−7), gradually displacing the equilibrium away from the Nbs' binding. In contrast, anti–IL-13 mAbs that have been tested in clinical trials all displayed much stronger affinity for IL-13 than the receptor subunit they were competing with. Tralokinumab, IMA-036, and cendakimab (RPC4046), which prevent the binding of IL-13 to $IL-13R_{\alpha 1}$, have a K_D of 165 pM (16), 92 pM (66), and 50 pM (67), respectively, and so are well beyond the affinity of IL-13 for $IL-13R_{\alpha 1}$ (2−10 nM) (3−6). Anti–IL-13 mAbs preventing the binding of the primary complex to IL-4R (anrunkinzumab and lebrikizumab) displayed even lower K_Ds [14 pM (66) and below 10 pM (60), respectively] as the complete IL-13/receptors complex ($IL13R\alpha 1$/IL-13/IL-4R) K_D was itself lower (32−400 pM) (5−7).

Moreover, with IL-binding Nb, the expected tissue concentration is very low, even for an overexpressed target. For comparison, concentrations of IL-13 in sputum from patients with mild, moderate, and severe asthma were below 1 ng/g of sputum (89). It is therefore likely that IL-13 concentrations in those population lungs would be approximately equal to or below what was used in the cell-based assay (0.5 ng/ml ≈ 40 pM). However, the potency ceiling of Abs and derivatives states that for Ag concentrations below the K_D, the binding will be mainly driven by the affinity of the Ab. When the Ag concentration is equal to or above the Ab K_D, the binding becomes purely stochiometric, and further improvement regarding the K_D does not usually lead to concomitant inhibitory activity improvement (90). In our cell-based assay and in asthmatic patient sputum, the final concentration of IL-13 would therefore be between 40 and 80 pM, which is far below the K_D of any of the monomeric or multimeric Nbs. It is thereby likely that improving their intrinsic affinity, if possible, would improve the binding efficiency and their potency. The typical affinity range that can be reached with monomeric Nbs after affinity maturation is in the midpicomolar range (91), but midfemtomolar range (0.19 pM) has also been reported (80). Higher affinity can then be obtained by multimerizing the monomeric constructs.

In conclusion, this study showed that Nbs can be engineered into multimeric constructs to significantly enhance their antagonistic activity, transforming poorly active monomers into moderately active multimers. Although picomolar IC_{50} were not obtained as for the already available anti–IL-13 mAbs, the nature of Nbs allow much space for enhancing their therapeutic efficacy over conventional mAbs (i.e., linking to other subunits targeting the same or another target and using different types of linkers). Finally, these lower m.w. and recognized higher stability over conventional mAbs would especially be important for diseases in which local administration is the cornerstone of therapy, such as asthma. This way, Nbs permit therapeutic strategies that are poorly effective when using intact conventional mAbs to meet unmet needs.

Disclosures

References

1. UniProt Consortium. UniProtKB - P35225 (IL13_HUMAN). UniProt. Available at: https://www.uniprot.org/uniprot/P35225. Accessed: October 14, 2020.
2. Minty, A., P. Chalon, J. M. Derocq, X. Dumont, J. C. Guillemot, M. Kaghad, C. Labit, P. Leplatois, P. Liauzun, B. Miloux, et al. 1993. Interleukin-13 is a new human lymphokine regulating inflammatory and immune responses. *Nature.* 362: 248–250.
3. Wills-Karp, M. 2004. Interleukin-13 in asthma pathogenesis. *Curr. Allergy Asthma Rep.* 4: 123–131.
4. Lupardus, P. J., M. E. Birnbaum, and K. C. Garcia. 2010. Molecular basis for shared cytokine recognition revealed in the structure of an unusually high affinity complex between IL-13 and IL-13Ralpha2. *Structure.* 18: 332–342.
5. Hilton, D. J., J. G. Zhang, D. Metcalf, W. S. Alexander, N. A. Nicola, and T. A. Willson. 1996. Cloning and characterization of a binding subunit of the interleukin 13 receptor that is also a component of the interleukin 4 receptor. *Proc. Natl. Acad. Sci. USA.* 93: 497–501.
6. Miloux, B., P. Laurent, O. Bonnin, J. Lupker, D. Caput, N. Vita, and P. Ferrara. 1997. Cloning of the human IL-13R α1 chain and reconstitution with the IL4R α of a functional IL-4/IL-13 receptor complex. *FEBS Lett.* 401: 163–166.
7. Aman, M. J., N. Tayebi, N. I. Obiri, R. K. Puri, W. S. Modi, and W. J. Leonard. 1996. cDNA cloning and characterization of the human interleukin 13 receptor α chain. *J. Biol. Chem.* 271: 29265–29270.
8. Mak, T. W., and M. E. Saunders. 2006. Cytokines and cytokine receptors. In *The Immune Response*, 1st Ed. T. W. Mak and M. E. Saunders, eds. Academic Press, Cambridge, MA, p. 463–516.
9. O'Shea, J. J., M. Gadina, and M. Richard Siegel. 2019. Cytokines and cytokine receptors. In *Clinical Immunology*, 5th Ed. vol. 1. R. R. Rich, T. A. Fleisher, W. T. Shearer,

H. W. Schroeder, A. J. Frew, and C. M. Weyand, eds. Elsevier, Amsterdam, the Netherlands, p. 127–155.

10. Fichtner-Feigl, S., W. Strober, K. Kawakami, R. K. Puri, and A. Kitani. 2006. IL-13 signaling through the IL-13α2 receptor is involved in induction of TGF-β1 production and fibrosis. *Nat. Med.* 12: 99–106.

11. Rahaman, S. O., P. Sharma, P. C. Harbor, M. J. Aman, M. A. Vogelbaum, and S. J. Haque. 2002. IL-13R(α)2, a decoy receptor for IL-13 acts as an inhibitor of IL-4-dependent signal transduction in glioblastoma cells. *Cancer Res.* 62: 1103–1109.

12. Wills-Karp, M., J. Luyimbazi, X. Xu, B. Schofield, T. Y. Neben, C. L. Karp, and D. D. Donaldson. 1998. Interleukin-13: central mediator of allergic asthma. *Science.* 282: 2258–2261.

13. Hansbro, P. M., G. E. Kaiko, and P. S. Foster. 2011. Cytokine/anti-cytokine therapy - novel treatments for asthma? *Br. J. Pharmacol.* 163: 81–95.

14. Yang, G., L. Li, A. Volk, E. Emmell, J. Petley, J. Giles-Komar, P. Rafferty, M. Lakshminarayanan, D. E. Griswold, P. J. Bugelski, and A. M. Das. 2005. Therapeutic dosing with anti-interleukin-13 monoclonal antibody inhibits asthma progression in mice. *J. Pharmacol. Exp. Ther.* 313: 8–15.

15. Hacha, J., K. Tomlinson, L. Maertens, G. Paulissen, N. Rocks, J. M. Foidart, A. Noel, R. Palframan, M. Gueders, and D. D. Cataldo. 2012. Nebulized anti-IL-13 monoclonal antibody Fab' fragment reduces allergen-induced asthma. *Am. J. Respir. Cell Mol. Biol.* 47: 709–717.

16. May, R. D., P. D. Monk, E. S. Cohen, D. Manuel, F. Dempsey, N. H. E. Davis, A. J. Dodd, D. J. Corkill, J. Woods, C. Joberty-Candotti, et al. 2012. Preclinical development of CAT-354, an IL-13 neutralizing antibody, for the treatment of severe uncontrolled asthma. *Br. J. Pharmacol.* 166: 177–193.

17. Oh, C. K., G. P. Geba, and N. Molfino. 2010. Investigational therapeutics targeting the IL-4/IL-13/STAT-6 pathway for the treatment of asthma. *Eur. Respir. Rev.* 19: 46–54.

18. Blanchard, C., A. Mishra, H. Saito-Akei, P. Monk, I. Anderson, and M. E. Rothenberg. 2005. Inhibition of human interleukin-13-induced respiratory and oesophageal inflammation by anti-human-interleukin-13 antibody (CAT-354). *Clin. Exp. Allergy* 35: 1096–1103.

19. Kumar, R. K., C. Herbert, D. C. Webb, L. Li, and P. S. Foster. 2004. Effects of anticytokine therapy in a mouse model of chronic asthma. *Am. J. Respir. Crit. Care Med.* 170: 1043–1048.

20. Suárez-Fariñas, M., N. Dhingra, J. Gittler, A. Shemer, I. Cardinale, C. de Guzman Strong, J. G. Krueger, and E. Guttman-Yassky. 2013. Intrinsic atopic dermatitis shows similar TH2 and higher TH17 immune activation compared with extrinsic atopic dermatitis. *J. Allergy Clin. Immunol.* 132: 361–370.

21. Jeong, C.-W., K.-S. Ahn, N.-K. Rho, Y.-D. Park, D.-Y. Lee, J.-H. Lee, E.-S. Lee, and J.-M. Yang. 2003. Differential in vivo cytokine mRNA expression in lesional skin of intrinsic vs. extrinsic atopic dermatitis patients using semiquantitative RT-PCR. *Clin. Exp. Allergy.* 33: 1717–1724.

22. Park, S.-W., M.-H. Ahn, H. K. Jang, A. S. Jang, D.-J. Kim, E.-S. Koh, J.-S. Park, S.-T. Uh, Y. H. Kim, J. S. Park, et al. 2009. Interleukin-13 and its receptors in idiopathic interstitial pneumonia: clinical implications for lung function. *J. Korean Med. Sci.* 24: 614–620.

23. Sui, G., G. Cheng, J. Yuan, X. Hou, X. Kong, and H. Niu. 2018. Interleukin (IL)-13, prostaglandin E2 (PGE2), and prostacyclin 2 (PGI2) activate hepatic stellate cells via protein kinase C (PKC) pathway in hepatic fibrosis. *Med. Sci. Monit.* 24: 2134–2141.

24. Riccieri, V., T. Rinaldi, A. Spadaro, R. Scrivo, F. Ceccarelli, M. D. Franco, E. Taccari, and G. Valesini. 2003. Interleukin-13 in systemic sclerosis: relationship to nailfold capillaroscopy abnormalities. *Clin. Rheumatol.* 22: 102–106.

25. Gonçalves, R. S. G., M. C. Pereira, A. T. Dantas, A. R. de Almeida, M. J. B. M. Rego, E. A. Lima, I. d. R. Pitta, A. L. B. P. Duarte, and M. G. D. R. Pitta. 2019. CCL3, IL-7, IL-13 and IFNγ transcripts are increased in skin's biopsy of systemic sclerosis. *Exp. Dermatol.* 28: 1172–1175.

26. Granel, B., Y. Allanore, C. Chevillard, V. Arnaud, S. Marquet, P.-J. Weiller, J.-M. M. Durand, J.-R. R. Harlé, C. Grange, Y. Frances, et al. 2006. IL13RA2 gene polymorphisms are associated with systemic sclerosis. *J. Rheumatol.* 33: 2015–2019.

27. Fuss, I. J., F. Heller, M. Boirivant, F. Leon, M. Yoshida, S. Fichtner-Feigl, Z. Yang, M. Exley, A. Kitani, R. S. Blumberg, et al. 2004. Nonclassical CD1d-restricted NK T cells that produce IL-13 characterize an atypical Th2 response in ulcerative colitis. *J. Clin. Invest.* 113: 1490–1497.

28. Blanchard, C., M. K. Mingler, M. Vicario, J. P. Abonia, Y. Y. Wu, T. X. Lu, M. H. Collins, P. E. Putnam, S. I. Wells, and M. E. Rothenberg. 2007. IL-13 involvement in eosinophilic esophagitis: transcriptome analysis and reversibility with glucocorticoids. *J. Allergy Clin. Immunol.* 120: 1292–1300.

29. Zuo, L., P. C. Fulkerson, F. D. Finkelman, M. Mingler, C. A. Fischetti, C. Blanchard, and M. E. Rothenberg. 2010. IL-13 induces esophageal remodeling and gene expression by an eosinophil-independent, IL-13R α 2-inhibited pathway. *J. Immunol.* 185: 660–669.

30. Terabe, M., S. Matsui, J.-M. Park, M. Mamura, N. Noben-Trauth, D. D. Donaldson, W. Chen, S. M. Wahl, S. Ledbetter, B. Pratt, et al. 2003. Transforming growth factor-β production and myeloid cells are an effector mechanism through which CD1d-restricted T cells block cytotoxic T lymphocyte-mediated tumor immunosurveillance: abrogation prevents tumor recurrence. *J. Exp. Med.* 198: 1741–1752.

31. Mak, T. W., and M. E. Saunders. 2006. Hematopoietic Cancers. In *The Immune Response,* 1st Ed. T. W. Mak and M. E. Saunders, eds. Academic Press, Cambridge, MA, p. 1025–1063.

32. Skinnider, B. F., A. J. Elia, R. D. Gascoyne, L. H. Trümper, F. von Bonin, U. Kapp, B. Patterson, B. E. Snow, and T. W. Mak. 2001. Interleukin 13 and interleukin 13 receptor are frequently expressed by Hodgkin and Reed-Sternberg cells of Hodgkin lymphoma. *Blood.* 97: 250–255.

33. Kapp, U., W.-C. Yeh, B. Patterson, A. J. Elia, D. Kägi, A. Ho, A. Hessel, M. Tipsword, A. Williams, C. Mirtsos, et al. 1999. Interleukin 13 is secreted by and stimulates the growth of Hodgkin and Reed-Sternberg cells. *J. Exp. Med.* 189: 1939–1946.

34. Rothenberg, M. E., T. Wen, A. Greenberg, O. Alpan, B. Enav, I. Hirano, K. Nadeau, S. Kaiser, T. Peters, A. Perez, et al. 2015. Intravenous anti-IL-13 mAb QAX576 for the treatment of eosinophilic esophagitis. *J. Allergy Clin. Immunol.* 135: 500–507.

35. Straumann, A., S. Conus, P. Grzonka, H. Kita, G. Kephart, C. Bussmann, C. Beglinger, D. A. Smith, J. Patel, M. Byrne, and H.-U. Simon. 2010. Anti-interleukin-5 antibody treatment (mepolizumab) in active eosinophilic oesophagitis: a randomised, placebo-controlled, double-blind trial. *Gut.* 59: 21–30.

36. Hirano, I., M. H. Collins, Y. Assouline-Dayan, L. Evans, S. Gupta, A. M. Schoepfer, A. Straumann, E. Safroneeva, M. Grimm, H. Smith, et al; HEROES Study Group. 2019. RPC4046, a monoclonal antibody against IL13, reduces histologic and endoscopic activity in patients with eosinophilic esophagitis. *Gastroenterology.* 156: 592–603.e10.

37. Korenblat, P., E. Kerwin, I. Leshchenko, K. Yen, C. T. J. Holweg, J. Anzures-Cabrera, C. Martin, W. S. Putnam, L. Governale, J. Olsson, and J. G. Matthews. 2018. Efficacy and safety of lebrikizumab in adult patients with mild-to-moderate asthma not receiving inhaled corticosteroids. *Respir. Med.* 134: 143–149.

38. Hanania, N. A., P. Korenblat, K. R. Chapman, E. D. Bateman, P. Kopecky, P. Paggiaro, A. Yokoyama, J. Olsson, S. Gray, C. T. J. Holweg, et al. 2016. Efficacy and safety of lebrikizumab in patients with uncontrolled asthma (LAVOLTA I and LAVOLTA II): replicate, phase 3, randomised, double-blind, placebo-controlled trials. *Lancet Respir. Med.* 4: 781–796.

39. Gauvreau, G. M., L.-P. P. Boulet, D. W. Cockcroft, J. M. Fitzgerald, C. Carlsten, B. E. Davis, F. Deschesnes, M. Duong, B. L. Durn, K. J. Howie, et al. 2011. Effects of interleukin-13 blockade on allergen-induced airway responses in mild atopic asthma. *Am. J. Respir. Crit. Care Med.* 183: 1007–1014.

40. Pfizer. 2015. Study evaluating the effect of IMA-638 in subjects with persistent asthma. In: ClinicalTrials.gov. National Library of Medicine (US), Bethesda, MD. NLM Identifier: NCT00425061. Available at: https://clinicaltrials.gov/ct2/show/results/NCT00425061?term=IMA638&draw=2&rank=3. Accessed: July 27, 2020.

41. Novartis Pharmaceuticals. 2020. Efficacy of QAX576 in asthma. In: Clinical-Trials.gov. National Library of Medicine (US), Bethesda, MD. NLM Identifier: NCT01130064. Available at: https://clinicaltrials.gov/ct2/show/NCT01130064. Accessed: June 12, 2020.

42. Panettieri, R. A., Jr., U. Sjöbring, A. Péterffy, P. Wessman, K. Bowen, E. Piper, G. Colice, and C. E. Brightling. 2018. Tralokinumab for severe, uncontrolled asthma (STRATOS 1 and STRATOS 2): two randomised, double-blind, placebo-controlled, phase 3 clinical trials. *Lancet Respir. Med.* 6: 511–525.

43. Parker, J. M., I. N. Glaspole, L. H. Lancaster, T. J. Haddad, D. She, S. L. Roseti, J. P. Fiening, E. P. Grant, C. M. Kell, and K. R. Flaherty. 2018. A phase 2 randomized controlled study of tralokinumab in subjects with idiopathic pulmonary fibrosis. *Am. J. Respir. Crit. Care Med.* 197: 94–103.

44. Danese, S., J. Rudziński, W. Brandt, J. L. Dupas, L. Peyrin-Biroulet, Y. Bouhnik, D. Kleczkowski, P. Uebel, M. Lukas, M. Knutsson, et al. 2015. Tralokinumab for moderate-to-severe UC: a randomised, double-blind, placebo-controlled, phase IIa study. *Gut* 64: 243–249.

45. E. Gutman. 2020. A pilot study of tralokinumab in subjects with moderate to severe alopecia areata. In: ClinicalTrials.gov. National Library of Medicine (US), Bethesda, MD. NLM Identifier: NCT02684097. Available at: https://clinicaltrials.gov/ct2/show/results/NCT02684097?term=tralokinumab&phase=1&draw=2&rank=1. Accessed: January 30, 2020.

46. Reinisch, W., J. Panés, S. Khurana, G. Toth, F. Hua, G. M. Comer, M. Hinz, K. Page, M. O'Toole, T. M. D. Moorehead, et al. 2015. Anrukinzumab, an anti-interleukin 13 monoclonal antibody, in active UC: efficacy and safety from a phase IIa randomised multicentre study. *Gut.* 64: 894–900.

47. Novartis Pharmaceuticals. 2020. Safety and efficacy of QAX576 in patients with idiopathic pulmonary fibrosis (IPF). In: ClinicalTrials.gov. National Library of Medicine (US), Bethesda, MD. NLM Identifier: NCT01266135. Available at: https://clinicaltrials.gov/ct2/show/NCT01266135. Accessed: June 12, 2020.

48. Novartis Pharmaceuticals. 2020. QAX576 in patients with pulmonary fibrosis secondary to systemic sclerosis. In: ClinicalTrials.gov. National Library of Medicine (US), Bethesda, MD. NLM Identifier: NCT00581997. Available at: https://clinicaltrials.gov/ct2/show/NCT00581997. Accessed: June 12, 2020.

49. Novartis Pharmaceuticals. 2020. Efficacy 2 part study of identification of keloid biomarkers and effect of QAX576 on keloid recurrence. In: ClinicalTrials.gov. National Library of Medicine (US), Bethesda, MD. NLM Identifier: NCT00987545. https://clinicaltrials.gov/ct2/show/NCT00987545. Accessed: June 12, 2020.

50. Costantino, H. R., J. D. Andya, P.-A. Nguyen, N. Dasovich, T. D. Sweeney, S. J. Shire, C. C. Hsu, and Y.-F. Maa. 1998. Effect of mannitol crystallization on the stability and aerosol performance of a spray-dried pharmaceutical protein, recombinant humanized anti-IgE monoclonal antibody. *J. Pharm. Sci.* 87: 1406–1411.

51. Andya, J. D., Y. F. Maa, H. R. Costantino, P. A. Nguyen, N. Dasovich, T. D. Sweeney, C. C. Hsu, and S. J. Shire. 1999. The effect of formulation excipients on protein stability and aerosol performance of spray-dried powders of a recombinant humanized anti-IgE monoclonal antibody. *Pharm. Res.* 16: 350–358.

52. Muyldermans, S. 2013. Nanobodies: natural single-domain antibodies. *Annu. Rev. Biochem.* 82: 775–797.

53. Hassanzadeh-Ghassabeh, G., N. Devoogdt, P. De Pauw, C. Vincke, and S. Muyldermans. 2013. Nanobodies and their potential applications. *Nanomedicine (Lond.).* 8: 1013–1026.

54. Ulrichts, H., K. Silence, A. Schoolmeester, P. de Jaegere, S. Rossenu, J. Roodt, S. Priem, M. Lauwereys, P. Casteels, F. Van Bockstaele, et al. 2011.

Antithrombotic drug candidate ALX-0081 shows superior preclinical efficacy and safety compared with currently marketed antiplatelet drugs. *Blood.* 118: 757–765.

55. Sanofi. Cablivi (caplacizumab) approved in Europe for adults with acquired thrombotic thrombocytopenic purpura (aTTP). Available at: http://hugin.info/152918/R/2213684/863478.pdf. Accessed: June 12, 2020.

56. Vincke, C., C. Gutiérrez, U. Wernery, N. Devoogdt, G. Hassanzadeh-Ghassabeh, and S. Muyldermans. 2012. Generation of single domain antibody fragments derived from camelids and generation of manifold constructs. In *Endeavour.* P. Chames, ed. Vol. 18. Humana Press, Totowa, NJ, p. 145–176.

57. Conrath, K. E., M. Lauwereys, M. Galleni, A. Matagne, J. M. Frère, J. Kinne, L. Wyns, and S. Muyldermans. 2001. Beta-lactamase inhibitors derived from single-domain antibody fragments elicited in the camelidae. *Antimicrob Agents Chemother.* 45: 2807–2812.

58. Zell, R., and H. J. Fritz. 1987. DNA mismatch-repair in *Escherichia coli* counteracting the hydrolytic deamination of 5-methyl-cytosine residues. *EMBO J.* 6: 1809–1815.

59. Schoonooghe, S., J. Leoen, and J. Haustraete. 2012. Production of antibody derivatives in the methylotrophic yeast Pichia pastoris. *Methods Mol. Biol.* 907: 325–340.

60. Ultsch, M., J. Bevers, G. Nakamura, R. Vandlen, R. F. Kelley, L. C. Wu, and C. Eigenbrot. 2013. Structural basis of signaling blockade by anti-IL-13 antibody lebrikizumab. *J. Mol. Biol.* 425: 1330–1339.

61. Kim, J.-E., K. Jung, J.-A. Kim, S.-H. Kim, H.-S. Park, and Y.-S. Kim. 2019. Engineering of anti-human interleukin-4 receptor alpha antibodies with potent antagonistic activity. *Sci. Rep.* 9: 7772.

62. Ahmed, N., P. Dhanapala, and C. Suphioglu. 2015. Identification and characterization of a novel IL-4 receptor α chain (IL-4Rα) antagonist to inhibit IL-4 signalling. *Cell. Physiol. Biochem.* 36: 831–842.

63. Duppatla, V., M. Gjorgjevikj, W. Schmitz, H. M. Hermanns, C. M. Schäfer, M. Kottmair, T. Müller, and W. Sebald. 2014. IL-4 analogues with site-specific chemical modification at position 121 inhibit IL-4 and IL-13 biological activities. *Bioconjug. Chem.* 25: 52–62.

64. Obmolova, G., A. Teplyakov, T. J. Malia, E. Keough, J. Luo, R. Sweet, S. A. Jacobs, F. Yi, R. Hippensteel, K. T. O'Neil, and G. L. Gilliland. 2015. Induced conformational change in human IL-4 upon binding of a signal-neutralizing DARPin. *Proteins.* 83: 1191–1197.

65. Chelius, D., K. Jing, A. Lueras, D. S. Rehder, T. M. Dillon, A. Vizel, R. S. Rajan, T. Li, M. J. Treuheit, and P. V. Bondarenko. 2006. Formation of pyroglutamic acid from N-terminal glutamic acid in immunoglobulin gamma antibodies. *Anal. Chem.* 78: 2370–2376.

66. Kasaian, M. T., X.-Y. Tan, M. Jin, L. Fitz, K. Marquette, N. Wood, T. A. Cook, J. Lee, A. Widom, R. Agostinelli, et al. 2008. Interleukin-13 neutralization by two distinct receptor blocking mechanisms reduces immunoglobulin E responses and lung inflammation in cynomolgus monkeys. *J. Pharmacol. Exp. Ther.* 325: 882–892.

67. Ying, H., R. Miller, S. Bose, M. Argiriadi, C. Cuff, and C. Wu. 2010. ABT-308, a highly potent anti-IL-13 therapeutic antibody for the treatment of human asthma. *Amer. J. Resp. Crit. Care Med.* 355: A6644.

68. Kasaian, M. T., and D. K. Miller. 2008. IL-13 as a therapeutic target for respiratory disease. *Biochem. Pharmacol.* 76: 147–155.

69. Peyrassol, X., T. Laeremans, M. Gouwy, V. Lahura, M. Debulpaep, J. Van Damme, J. Steyaert, M. Parmentier, and I. Langer. 2016. Development by genetic immunization of monovalent antibodies (nanobodies) behaving as antagonists of the human ChemR23 receptor. *J. Immunol.* 196: 2893–2901.

70. Detalle, L., T. Stohr, C. Palomo, P. A. Piedra, B. E. Gilbert, V. Mas, A. Millar, U. F. Power, C. Stortelers, K. Allosery, et al. 2015. Generation and characterization of ALX-0171, a potent novel therapeutic nanobody for the treatment of respiratory syncytial virus infection. *Antimicrob. Agents Chemother.* 60: 6–13.

71. Hultberg, A., N. J. Temperton, V. Rosseels, M. Koenders, M. Gonzalez-Pajuelo, B. Schepens, L. I. Ibañez, P. Vanlandschoot, J. Schillemans, M. Saunders, et al. 2011. Llama-derived single domain antibodies to build multivalent, superpotent and broadened neutralizing anti-viral molecules. *PLoS One.* 6: e17665.

72. Desmyter, A., S. Spinelli, C. Boutton, M. Saunders, C. Blachetot, H. de Haard, G. Denecker, M. Van Roy, C. Cambillau, and H. Rommelaere. 2017.

73. Vladich, F. D., S. M. Brazille, D. Stern, M. L. Peck, R. Ghittoni, and D. Vercelli. 2005. IL-13 R130Q, a common variant associated with allergy and asthma, enhances effector mechanisms essential for human allergic inflammation. *J. Clin. Invest.* 115: 747–754.

74. Hoefman, S., I. Ottevaere, J. Baumeister, and M. Sargentini-Maier. 2015. Preclinical intravenous serum pharmacokinetics of albumin binding and non-half-life extended nanobodies. *Antibodies (Basel).* 4: 141–156.

75. de Marco, A. 2020. Recombinant expression of nanobodies and nanobody-derived immunoreagents. *Protein Expr. Purif.* 172: 105645.

76. Yu, Q.-N., W.-P. Tan, X.-L. Fan, Y.-B. Guo, Z.-L. Qin, C.-L. Li, D. Chen, Z. B. Lin, W. Wen, and Q.-L. Fu. 2018. Increased group 2 innate lymphoid cells are correlated with eosinophilic granulocytes in patients with allergic airway inflammation. *Int. Arch. Allergy Immunol.* 176: 124–132.

77. Harmsen, M. M., and H. J. De Haard. 2007. Properties, production, and applications of camelid single-domain antibody fragments. *Appl. Microbiol. Biotechnol.* 77: 13–22.

78. Gupta, V., M. Sengupta, J. Prakash, and B. C. Tripathy. 2017. Production of Recombinant Pharmaceutical Proteins. In *Basic and Applied Aspects of Biotechnology*. V. Gupta, M. Sengupta, J. Prakash, and B. C. Tripathy, eds. Springer Singapore, Singapore, p. 77–101.

79. Bartunek, J., E. Barbato, G. Heyndrickx, M. Vanderheyden, W. Wijns, and J. B. Holz. 2013. Novel antiplatelet agents: ALX-0081, a nanobody directed towards von Willebrand factor. *J. Cardiovasc. Transl. Res.* 6: 355–363.

80. Van Roy, M., C. Ververken, E. Beirnaert, S. Hoefman, J. Kolkman, M. Vierboom, E. Breedveld, B. 't Hart, S. Poelmans, L. Bontinck, et al. 2015. The preclinical pharmacology of the high affinity anti-IL-6R Nanobody® ALX-0061 supports its clinical development in rheumatoid arthritis. *Arthritis Res. Ther.* 17: 135.

81. Elsadek, B., and F. Kratz. 2012. Impact of albumin on drug delivery–new applications on the horizon. *J. Control. Release* 157: 4–28.

82. Schoen, P., S. Jacobs, K. Verschueren, I. Ottevaere, S. Sobry, and J.-B. Holz. 2013. Anti-RANKL nanobody ALX-0141 shows sustained biomarker inhibition in a phase I study in healthy postmenopausal women. *Bone Abstr.* 1: PP135.

83. Vanheusden, K., L. Detalle, A. Hemeryck, A. Vicari, R. Grenningloh, S. Poelmans, H. Wouters, and T. Stohr. 2013. Pre-clinical proof-of-concept of ALX-0761, a nanobody neutralizing both IL-17a and f in a cynomolgus monkey collagen induced arthritis model. *Arthritis Rheum.* 65: S543.

84. Newcomb, D. C., and R. S. Peebles, Jr. 2013. Th17-mediated inflammation in asthma. *Curr. Opin. Immunol.* 25: 755–760.

85. Staton, T. L., K. Peng, R. Owen, D. F. Choy, C. R. Cabanski, A. Fong, F. Brunstein, K. R. Alatsis, and H. Chen. 2019. A phase I, randomized, observer-blinded, single and multiple ascending-dose study to investigate the safety, pharmacokinetics, and immunogenicity of BITS7201A, a bispecific antibody targeting IL-13 and IL-17, in healthy volunteers. *BMC Pulm. Med.* 19: 5.

86. Venkataramani, S., S. Low, B. Weigle, D. Dutcher, K. Jerath, M. Menzenski, L. Frego, K. Truncali, P. Gupta, R. Kroe-Barrett, et al. 2018. Design and characterization of Zweimab and Doppelmab, high affinity dual antagonistic anti-TSLP/IL13 bispecific antibodies. *Biochem. Biophys. Res. Commun.* 504: 19–24.

87. Shah, D. K., and A. M. Betts. 2013. Antibody biodistribution coefficients: inferring tissue concentrations of monoclonal antibodies based on the plasma concentrations in several preclinical species and human. *MAbs* 5: 297–305.

88. Van Heeke, G., K. Allosery, V. De Brabandere, T. De Smedt, L. Detalle, and A. de Fougerolles. 2017. Nanobodies® as inhaled biotherapeutics for lung diseases. *Pharmacol. Ther.* 169: 47–56.

89. Saha, S. K., M. A. Berry, D. Parker, S. Siddiqui, A. Morgan, P. May, P. Monk, P. Bradding, A. J. Wardlaw, I. D. Pavord, and C. E. Brightling. 2008. Increased sputum and bronchial biopsy IL-13 expression in severe asthma. *J. Allergy Clin. Immunol.* 121: 685–691.

90. Tabrizi, M. A., G. G. Bornstein, S. L. Klakamp. 2018. *Development of Antibody-Based Therapeutics*. Springer Singapore, Singapore.

91. Beirnaert, E., A. Desmyter, S. Spinelli, M. Lauwereys, L. Aarden, T. Dreier, R. Loris, K. Silence, C. Pollet, C. Cambillau, and H. de Haard. 2017. Bivalent llama single-domain antibody fragments against tumor necrosis factor have picomolar potencies due to intramolecular interactions. *Front. Immunol.* 8: 867.